

Weakly Supervised Camouflaged Object Detection Based on the SAM Model and Mask Guidance

Xia Li^{a,1}, Xinran Liu^{a,2}, Lin Qi^{a,*,3} and Junyu Dong^{a,4}

^aSchool of Computer Science and Technology, Ocean University of China, Qingdao 266100, China

ARTICLE INFO

Keywords:

Camouflaged object detection
Weak supervision
Segment anything model
Mask guidance

ABSTRACT

Camouflaged object detection (COD) from a single image is a challenging task due to the high similarity between objects and their surroundings. Existing fully supervised methods require labor-intensive pixel-level annotations, making weakly supervised methods a viable compromise that balances accuracy and annotation efficiency. However, weakly supervised methods often experience performance degradation due to the use of coarse annotations. In this paper, we introduce a new weakly supervised approach for camouflaged object detection to overcome these limitations. Specifically, we propose a novel network, MGNet, which tackles edge ambiguity and missed detections by utilizing initial masks generated by our custom-designed Cascaded Mask Decoder (CMD) to guide the segmentation process and enhance edge predictions. We introduce a Context Enhancement Module (CEM) to reduce the missing detection, and a Mask-guided Feature Aggregation Module (MFAM) for effective feature aggregation. For the weak supervision challenge, we propose BoxSAM, which leverages the Segment Anything Model (SAM) with bounding-box prompts to generate pseudo-labels. By employing a redundant processing strategy, high quality pixel-level pseudo-labels are provided for training MGNet. Extensive experiments demonstrate that our method delivers competitive performance against current state-of-the-art methods.

1. Introduction

Camouflaged object detection (COD) refers to the pixel-level segmentation of objects that blend seamlessly with their surrounding environment [8]. This task presents greater challenges compared to general object detection and salient object detection (SOD) because camouflaged objects usually make themselves highly match their surroundings in terms of texture, color and shape. The detection of camouflaged objects finds extensive utility in various practical domains such as polyp segmentation [10] in the medical domain, pest detection [11] in agriculture and object surface defect detection in the industrial field [9].

Benefiting from the strong learning capacity of advanced CNN and transformer architectures, COD has achieved remarkable progress in recent years. The task of COD has evolved from relying on low-level visual features, such as traditional texture [43], gradient [39], and motion features [17], to extracting high-level semantic features using deep learning methods. Recently, numerous deep learning-based methods for COD have achieved significant advancements [19, 18, 33, 15]. However, our experiments reveal that these methods still exhibit two shortcomings: 1) the ambiguous edges of camouflaged objects. 2) the missed detection of camouflaged objects. As shown in Figure 1, due to the intrinsic similarity between the camouflaged objects and the backgrounds, FSPNet [19] fails to completely detect the edges of caddis moth (row 1) and fish (row 2), and even misses the small hippocampi (rows 3 and 4).

In addition to these two problems, fully supervised COD training typically relies on pixel-level supervision,

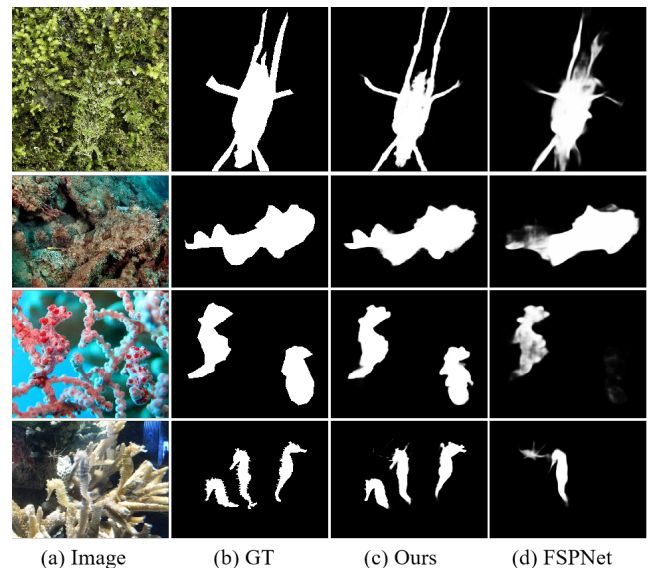


Figure 1: Visual examples of different methods. (a) RGB images. (b) Ground truth. (c)-(d) The detection results obtained by (c) Our results, (d) FSPNet [19].

which involves costly pixel-level annotation [1]. Consequently, weakly supervised COD holds significant research importance. Weakly supervised camouflaged object detection (WSCOD) relies on point annotations, bounding-box annotations or scribble annotations in the foreground or background, eliminating the need for pixel-level labeling. This approach enhances labeling efficiency and reduces costs. However, coarse annotations that only differentiate between foreground and background result in degraded segmentation performance. For instance, WSCOD based on scribble annotations [16] results in decreased segmentation

*Corresponding author

✉ 1x7211@stu.ouc.edu.cn (X. Li); 1xr7766@stu.ouc.edu.cn (X. Liu); qilin@ouc.edu.cn (L. Qi); dongjunyu@ouc.edu.cn (J. Dong)

accuracy. In addition, the community of weakly supervised salient object detection [66, 63, 29, 34, 47, 32] has made remarkable advancements, whereas there have been only very few attempts in WSCOD [16, 14, 4]. How to balance accuracy and annotation efficiency in WSCOD is still under exploration.

Inspired by the process of human observation, we first roughly localize the position and contour of the camouflaged object and then refine its edges. We propose the Mask-guided Network (MGNet) for the COD task, which guides subsequent segmentation through the initial generated masks by our designed Cascaded Mask Decoder (CMD). Specifically, to reduce the missing detection, we design a Context Enhancement Module (CEM), which employs convolutional layers with varying dilation rates to reduce information loss during the downsampling process. Besides, the CMD incrementally fuses multi-scale features, including high-level semantic information and low-level detail information, to guide subsequent segmentation from a global perspective. To address the ambiguous edges problem, we design a Mask-guided Feature Aggregation Module (MFAM), which is utilized to identify the fine regions of objects by fusing adjacent-level features with the guidance of masks from the CMD.

To address the challenge of weak supervision, we propose BoxSAM. We annotate the images with bounding boxes, which are less affected by human subjective factors compared to scribble annotations and point annotations. This is attributable to the fact that both the position of the point annotations and the length and location of the scribble annotations can significantly impact the performance of the model. In contrast, under ideal circumstances, a bounding box annotation represents the minimal enclosing box that completely encompasses the object. Segment Anything Model (SAM) [25] possesses powerful segmentation capabilities, but its performance in the field of camouflaged object detection is not particularly outstanding due to the high intrinsic similarity between the camouflaged objects and the backgrounds, segmentation results of SAM may mistakenly classify the backgrounds as camouflaged objects [22, 45, 23]. To address this issue, we design a redundancy processing strategy to refine the initial labels, providing high-quality pixel-level pseudo labels for training MGNet. In contrast to the strategies during the training period [31], we directly process the pseudo-labels generated by SAM based on the bounding-box prompts. We propose the redundancy processing strategy specifically designed to address the issue of redundant predictions generated by SAM when segmenting images with cluttered backgrounds or scenarios where the background and camouflaged objects exhibit high similarity. By integrating deep learning model MGNet with the generalization capabilities of SAM, we achieve more accurate pseudo-label generation.

Our contributions in this paper are as follows:

- The proposed BoxSAM is a WSCOD method that generates pseudo-labels by annotating bounding-boxes of the camouflaged objects and integrating the SAM

model. Furthermore, we propose a redundancy processing strategy to obtain more accurate pseudo-labels.

- We propose a novel Mask-guided Network (MGNet) that enhances subsequent segmentation by utilizing the initially generated masks as guidance. We propose a CEM to reduce the missing detection. Additionally, we design a MFAM to aggregate features at different levels under the guidance of masks generated by the CMD.
- BoxSAM is evaluated on three widely used COD datasets, the experiments demonstrate that our method achieves state-of-the-art performance. MGNet outperforms the current state-of-the-art COD methods. In addition, it also demonstrates excellent performance in COD-related applications.

2. Related work

2.1. Camouflaged object detection

Traditional COD methods are susceptible to noise, resulting in relatively poor detection performance. With the advancement of deep learning, many contemporary COD methods now leverage deep learning techniques. Fan et al. [8] simulated the hunting process and proposed SINet, which initially searched for the disguised objects through the receptive field module, and then detected them through part of the decoder component and the search attention module. Similarly, Mei et al. [38] imitated the natural predation process to locate potential objects in a global perspective, and then used the focusing module for recognition to gradually refine the initial predictions by focusing on the blurred regions. Liu et al. [30] designed a region search module to mimic predator behavior to locate potential object regions, enhancing object location detection. Ye et al. [61] designed a diverse feature enhancement module that simulates the correspondingly expanded receptive fields of the human visual system by using convolutional kernels with different dilation rates in parallel. Pang et al. [40] proposed an effective unified collaborative pyramid network, which emulates the way humans behave when they view unclear images and videos, specifically the action of magnifying and reducing the view.

Some methods introduce additional priors. Xu et al. [55] explored semantic clues based on edge truth values and combined edge features with semantic features through an edge-guided fusion module. However, in a complex environment, the boundary leads to noise. To address this, Ji et al. [21] utilized a gradient-guided transfer module to aggregate multi-source features. Liu et al. [33] designed a Dense Interactive Decoder module that produces a rough localization map to enhance subsequent fusion features for more accurate detection. Yue et al. [65] focused on object regions and edges for detecting camouflaged objects in a coarse-to-fine manner.

Zhao et al. [71] proposed a denoising diffusion model to investigate how generative models can enhance the detection

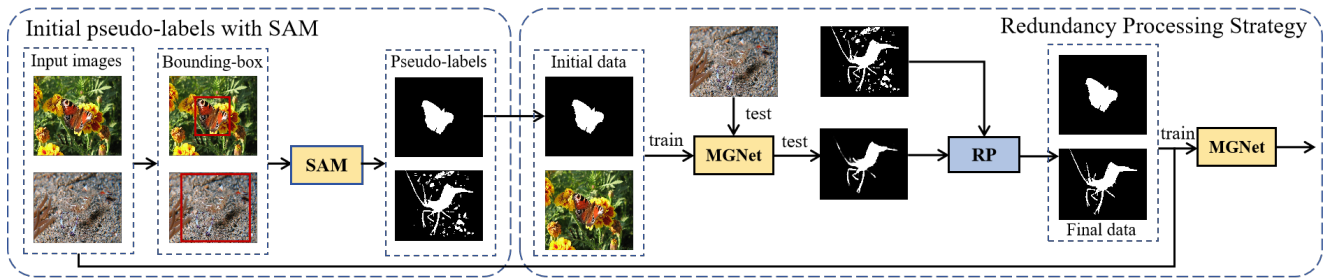


Figure 2: Overview of WSCOD with bounding-box supervision (BoxSAM). By annotating the bounding-boxes of the camouflaged objects and combining the SAM [25] model to output the pseudo-labels, we design a redundancy processing strategy (see Section 3.2) with MGNet (see Section 3.3) to process the pseudo-labels.

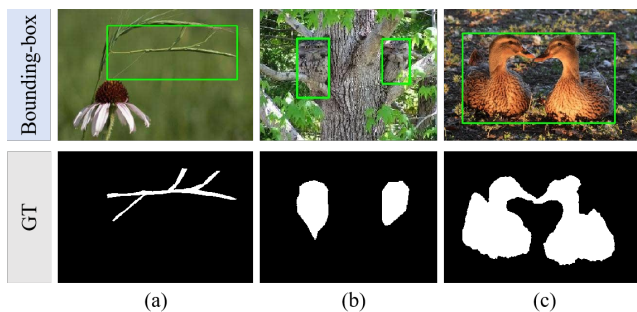


Figure 3: Bounding-box annotations method, images from CAMO [26] and COD10K [8]. The green bounding-boxes represent our annotated bounding-boxes. The annotations are classified into 3 cases: (a) A bounding-box contains a camouflaged object. (b) Multiple bounding-boxes contain multiple camouflaged objects. (c) A bounding-box contains multiple camouflaged objects.

and interpretation of camouflaged objects. DiffCOD [6] is also based on the diffusion model, which regards the task of COD as a denoising diffusion process which progresses from noisy masks to object masks. In addition, many scholars have also explored multi-image collaborative methods. Yu et al. [64] proposed DSAM by combining depth maps. They utilized the zero-shot capability of SAM to realize precise segmentation in the RGB-D domain. From the perspective of multi-scale context aggregation, He et al. [14] designed a multi-scale feature grouping module that first groups features at different granularities and then aggregates these grouping results. For high-resolution dichotomous image segmentation, Zheng et al. [72] proposed a novel bilateral reference framework (BiRefNet), which achieved excellent segmentation results in the COD task.

Existing methods for COD have demonstrated good performance. However, issues such as the missing detection and edge ambiguity persist, as illustrated in Figure 1. To address these issues, we design a Mask-guided Network (MGNet) that guides subsequent segmentation through the initial generated masks.

2.2. Weakly supervised COD

To balance labeling costs with detection performance, many researchers have turned to WSCOD. He et al. [16] proposed the first WSCOD framework, though its segmentation

performance is limited by the sparse information provided by scribble annotations. With the advent of large models, He et al. [14] proposed a WSCOD method leveraging a large model. This approach inputs images with scribble annotations into Segment Anything Model (SAM) [25], employing multiple enhancement result integration, entropy-based pixel-level weighting and entropy-based image-level selection strategies to provide more accurate supervision for the segmentation model. Chen et al. [4] proposed SAM-COD, which is designed to accommodate arbitrary weakly supervised labels. Additionally, in terms of learning from noisy pseudo-labels, Liu et al. [31] proposed ADELE for semantic segmentation in the presence of noisy pixel-level annotations, which detects the beginning of the memorization phase separately for each category to adaptively correct noisy annotations during training and incorporates a regularization term.

Methods that rely on scribble supervision are influenced by human subjective factors, such as the position of the marker and the length of the scribble line, which can negatively impact the segmentation results. Compared to scribble annotations, the bounding-box annotations are more intuitive and concise, and are less influenced by subjective factors. Therefore, we implement WSCOD using bounding-box annotations combined with SAM.

2.3. Weakly supervised SOD

SOD aims to segment regions that attract human attention [48], typically characterized by clearer edges compared to camouflaged objects. Research on weakly supervised SOD began earlier compared to WSCOD. Zhang et al. [66] utilized scribble annotations to learn saliency and designed a scribble enhancement scheme to iteratively refine these annotations, which were subsequently used to supervise the learning of high-quality saliency maps. To streamline training complexity, Yu et al. [63] devised SCWS, which is an end-to-end training approach for predicting comprehensive salient regions with complete object structures. This method propagates labels to unlabeled regions using image features and pixel distances, eliminating the need for preprocessing, post-processing, and extra supervised data. Addressing coarse annotated semantic segmentation, Liang et al. [29] introduced a tree energy loss mechanism that offers semantic guidance to unlabeled pixels.

In addition to scribble annotations, bounding-box annotations are utilized in weakly supervised SOD. Liu et al. [34] predicted the pixel-level pseudo ground truth saliency map using saliency bounding-boxes, generated initial saliency maps via an unsupervised SOD method, and iteratively refined the initial pseudo ground truth through a multi-task graph refinement network. Wang et al. [47] integrated bounding-box labels with the GrabCut algorithm to produce the initial saliency map and devise a correction module to enhance it. Liu et al. [32] employed bounding-box and SAM to generate the initial pseudo-labels, applying various strategies to enhance the segmentation accuracy of this map. Liu et al. [35] designed modal-aware modulators to extract modality-specific knowledge and a siamese decoder to address the discrepancy between training with scribble prompts and testing without prompts.

Due to the strong segmentation capabilities of SAM, it is frequently employed in image segmentation tasks [69, 3]. However, SAM faces significant challenges in camouflaged object detection task. Extensive experiments have demonstrated that SAM encounters challenges in accurately segmenting camouflaged objects [22], often misidentifying backgrounds as camouflaged objects, thereby introducing redundant information. To address this issue, we propose a redundancy processing strategy to enhance the performance of WSCOD.

3. Methodology

Figure 2 shows the pipeline of our proposed method, we propose a WSCOD method that utilizes bounding-box annotations as prompts in combination with SAM. In order to solve the problem of redundant information in the preliminary segmentation results, we develop a Redundancy Processing Strategy (RPS) that incorporates our designed Mask-guided Network (MGNet) which includes three proposed modules: the Cascaded Mask Decoder (CMD), the Context Enhancement Module (CEM) and the Mask-guided Feature Aggregation Module (MFAM). Detailed explanations of each component are provided in Sections 3.1–3.3.

3.1. Initial pseudo-labels with SAM

The Segment Anything Model (SAM) [25] is a newly introduced model for visual segmentation, trained with more than one billion segmentation masks. It has demonstrated exceptional performance in generating accurate segmentation masks across a broad range of object categories. SAM draws on the prompt strategy in the Natural Language Processing (NLP) field to complete the segmentation of arbitrary objects by providing prompts to the image segmentation task. It can be prompted by point annotations, scribble annotations and bounding-box annotations. In this paper, we use bounding-box annotations as prompts.

As shown in Figure 3, we annotate the bounding-boxes of the camouflaged objects according to the following rules [32]: 1) When an image only has a camouflaged object, the smallest bounding-box that encompasses the object is annotated, as shown in (a). 2) When an image has multiple

camouflaged objects, each object is annotated separately according to rule 1), as shown in (b). If there is overlap between multiple camouflaged objects, we merge them into a bounding-box, as shown in (c).

As shown in Figure 2, we first annotate the bounding-boxes of the camouflaged objects based on the above rules. Given a camouflaged image I with bounding-box B , we generate the initial pseudo-labels M with the bounding-boxes as prompts for the SAM model. This process can be formulated as Eq.1:

$$M = SAM(I, B) \quad (1)$$

where SAM denotes the Segment Anything Model [25].

3.2. Redundancy processing strategy

Due to the high similarity between the camouflaged objects and their backgrounds, SAM often mistakes the backgrounds for the camouflaged objects during segmentation [22], as shown in Figure 5. The quality of the labels significantly affects the model's performance, making it crucial to select accurate pseudo-labels. For each initial pseudo-label, the number of bounding-boxes is calculated following the rule of [32]. The pseudo-labels whose number of bounding-boxes is equal to the original annotation are used as the initial training data to train the MGNet, while those with mismatched numbers are denoted as F . The images corresponding to F are used as test data input to the already trained MGNet. To eliminate redundant information in the initial labels, we use the predicted masks to approximate the position and outline of the camouflaged objects. We save the predicted masks in image format according to [18, 7], denoted as the segmentation result P . To mitigate the redundant information present in F , we proposed a redundancy processing (RP) method. The following section provides a description of the RP method. The connected regions F_i of each F are counted. For each i , (m, n) represents the pixel coordinates in F_i . The corresponding region of F_i in P is determined by traversing $P(m, n)$. If the set of values of $P(m, n)$ contains non-zero values, the pixel values of $F(m, n)$ are set to 255. If all values in are 0, the pixel values of $F(m, n)$ are set to 0. This process can be formulated as Eq.2:

$$F(m, n) = \begin{cases} 255, & \exists(m, n) \in F_i, P(m, n) > 0, \\ 0, & \forall(m, n) \in F_i, P(m, n) = 0. \end{cases} \quad (2)$$

where (m, n) denotes the pixel coordinate. Finally, both the initial training dataset and the processed dataset are used to retrain MGNet. The whole process is shown in Figure 2.

3.3. Mask-guided network

3.3.1. Overall architecture

Figure 4 shows the structure of our proposed network. We select the Pyramid Visual Transformer (PVT) [49] as our feature extraction module. Specifically, for a given input image $I \in \mathbb{R}^{H \times W \times 3}$, PVTv2 [50] is used to encode the input image, obtaining multi-level features F_i ($i \in \{1, 2, 3, 4\}$) that contain rich spatial details and semantic information.

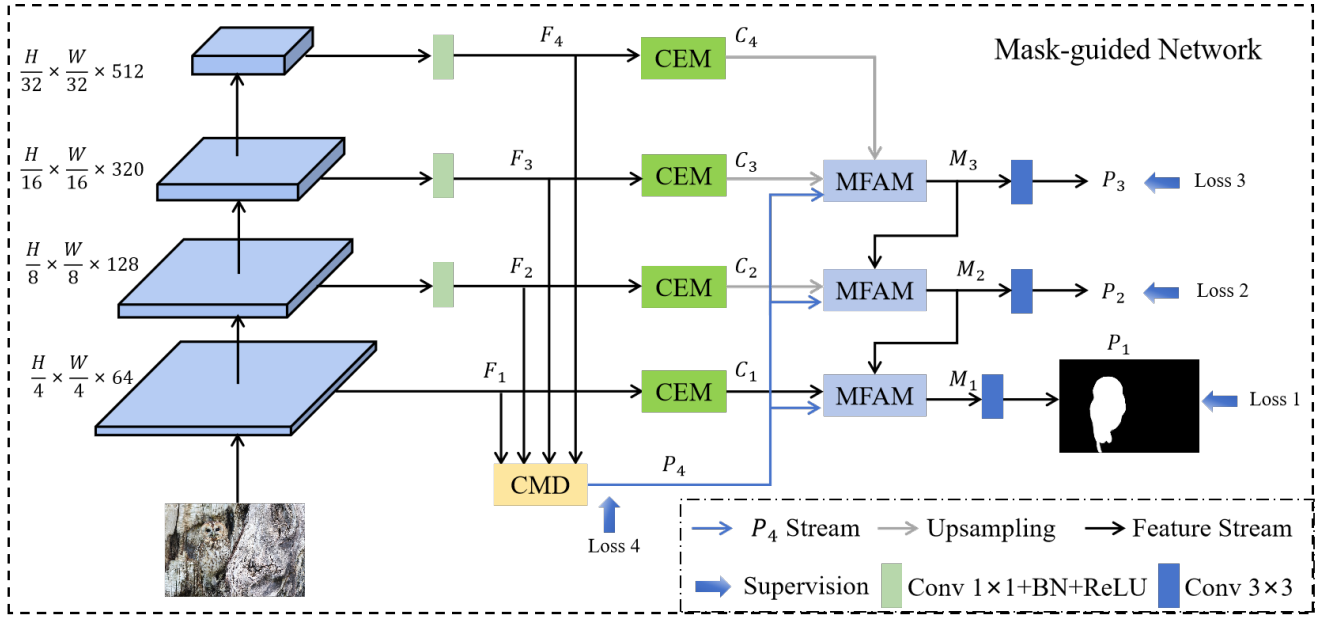


Figure 4: Overview of Mask-guided Network (MGNet). The MGNet consists of our designed Cascaded Mask Decoder (CMD, see Section 3.3.2), Context Enhancement Module (CEM, see Section 3.3.3) and Mask-guided Feature Aggregation Module (MFAM, see Section 3.3.4).

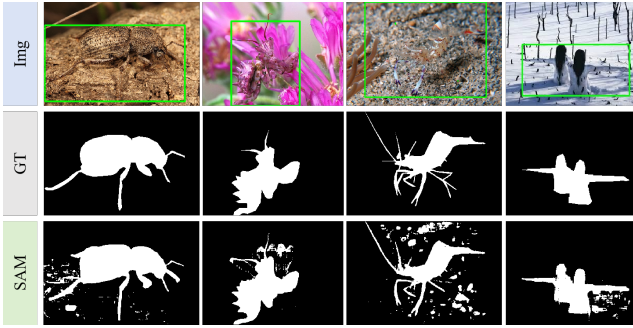


Figure 5: Some examples of SAM segmentation with bounding-boxes.

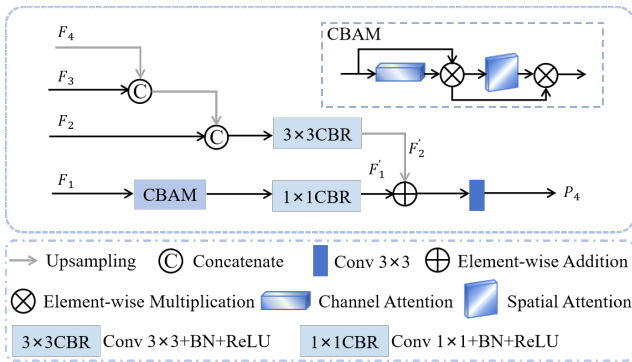


Figure 6: The details of Cascaded Mask Decoder (CMD).

The multi-level features are processed through the Cascaded Mask Decoder (CMD), which progressively integrates information from each layer to generate the mask P_4 . The multi-level features introduce rich context information through the Context Enhancement Module (CEM) to enhance feature

representation, resulting in C_i ($i \in \{1, 2, 3, 4\}$). Subsequently, under the guidance of mask P_4 , the Mask-guided Feature Aggregation Module (MFAM) aggregates different levels of features and outputs M_i ($i \in \{1, 2, 3\}$), where M_1 is used for the final output. Detailed explanations of each component are provided in Sections 3.3.2–3.3.4.

3.3.2. Cascaded mask decoder

In the task of COD, multi-scale information is believed to be important in distinguishing the targets from their surroundings [54]. To fully utilize information at different scales, we design the Cascaded Mask Decoder (CMD), as shown in Figure 6. This module gradually fuses multi-scale features through multi-level processing, integrating high-level semantic information and low-level detail information to generate an initial mask. The initial mask is subsequently used as input in the following steps to progressively refine the details of the camouflaged objects.

High-level semantic information is obtained through up-sampling and channel concatenation, resulting in the high-level feature F'_2 . To capture the details of the camouflaged objects from different dimensions, low-level information F_1 is processed using the Convolutional Block Attention Module (CBAM) [53] to obtain F'_1 . Finally, the mask P'_4 is obtained by summing F'_1 and F'_2 . This process can be formulated as Eq.3, Eq.4 and Eq.5:

$$F'_1 = \text{Conv}_1(\text{CBAM}(F_1)) \quad (3)$$

$$F'_2 = \text{Conv}_3(\text{cat}(\text{cat}(F_4 \uparrow, F_3) \uparrow, F_2)) \quad (4)$$

$$P'_4 = F'_1 + F'_2 \uparrow \quad (5)$$

where $\text{CBAM}(\cdot)$ denotes Convolutional Block Attention Module, \uparrow denotes the up-sampling, $\text{Conv}_1(\cdot)$ denotes a 1×1 convolution with batch normalization and ReLU. $\text{Conv}_3(\cdot)$

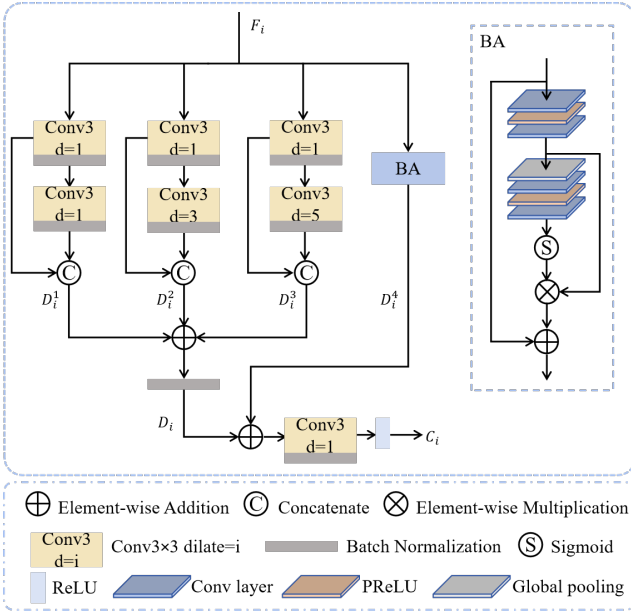


Figure 7: The details of Context Enhancement Module (CEM).

denotes a 3×3 convolution with batch normalization and ReLU. $cat(\cdot)$ represents the concatenation operation. The prediction mask P_4 can be obtained by processing P_4^j with a 3×3 convolution operation.

3.3.3. Context enhancement module

In the encoder stage, as the feature space is downsampled, this process poses the risk of losing details or missing camouflaged objects. To this end, we design the Context Enhancement Module (CEM), which employs convolutional layers with varying dilation rates [28] to expand the receptive field and introduce rich context information, thereby compensating for information loss during the downsampling process. Additionally, to further refine the details of camouflaged objects, we introduce the BA [18], which replaces ReLU with PReLU in Residual Channel Attention Block (RCAB) [68]. The BA focuses on extracting high-frequency information in the image and strengthens attention to details.

As illustrated in Figure 7, the CEM primarily consists of four branches. The first three branches each contain two 3×3 dilated convolutions, with each branch having a different dilation rate. The calculations for the first three branches are as Eq.6:

$$\begin{aligned} D_i^1 &= cat(Conv1(F_i), Conv1(Conv1(F_i))) \\ D_i^2 &= cat(Conv1(F_i), Conv3(Conv1(F_i))) \\ D_i^3 &= cat(Conv1(F_i), Conv5(Conv1(F_i))) \end{aligned} \quad (6)$$

where $Conv_d(\cdot)$ ($d \in \{1, 3, 5\}$) denotes a 3×3 convolutional layer and Batch Normalization, d is dilation rate. F_i ($i \in \{1, 2, 3, 4\}$) comes from the encoder and D_i^j ($j \in \{1, 2, 3\}$) is the result of the module's three feature mappings.

The final branch extracts high-frequency features using the BA to enhance attention to details. Subsequently, the

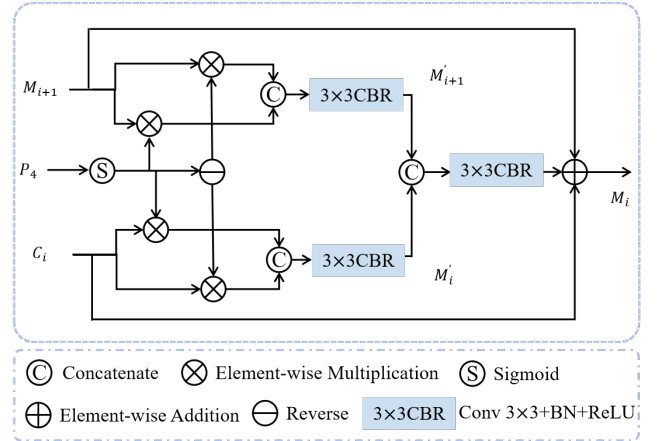


Figure 8: The details of Mask-guided Feature Aggregation Module (MFAM).

features from all four branches are combined and the features are extracted through a convolutional layer to obtain C_i , as expressed in the Eq. 7 and Eq. 8:

$$D_i = BN(D_i^1 + D_i^2 + D_i^3) \quad (7)$$

$$C_i = ReLU(Conv1(BA(F_i) + D_i)) \quad (8)$$

where $BN(\cdot)$ denotes Batch Normalization, $ReLU(\cdot)$ stands for Rectified Linear Unit. $BA(\cdot)$ represents the BA Block.

3.3.4. Mask-guided feature aggregation module

To achieve comprehensive multi-level feature fusion, we propose a Mask-guided Feature Aggregation Module (MFAM). As illustrated in Figure 8, this module effectively fuses features from top to bottom using masks generated by the Cascaded Mask Decoder (CMD). We extend P_4 to match the channel dimension of C_i ($i \in \{1, 2, 3\}$) through broadcasting. We apply P_4 to the sigmoid function to obtain the foreground attention map S_4 . Inspired by [70], we obtain the background attention map B_4 through the utilization of the inverse operation. The attention map is multiplied with the respective high-level and low-level features. By concatenating the results, we obtain two edge enhancement maps M'_{i+1} and M'_i . This process can be formulated as Eq.9, Eq.10, Eq.11 and Eq.12:

$$S_4 = \sigma(P_4) \quad (9)$$

$$B_4 = E - \sigma(P_4) \quad (10)$$

$$M'_{i+1} = Conv_3(cat(S_4 \otimes M_{i+1}, B_4 \otimes M_{i+1})) \quad (11)$$

$$M'_i = Conv_3(cat(S_4 \otimes C_i, B_4 \otimes C_i)) \quad (12)$$

where σ is the Sigmoid function, E denotes the matrix with all entries equal to one and \otimes denotes the element-wise multiplication. $Conv_3(\cdot)$ denotes a 3×3 convolution with batch normalization and the ReLU activation. $cat(\cdot)$ represents the concatenation operation. It is worth noting that when $i = 3$, M_4 represents C_4 .

After concatenating the high-level edge enhancement image M'_{i+1} with the low-level edge enhancement image

M'_i , element-wise summation of M_{i+1} and C_i is performed to retain the original important information. The above operations can be expressed as Eq.13:

$$M_i = \text{Conv}_3(\text{cat}(M'_{i+1}, M'_i)) + M_{i+1} + C_i \quad (13)$$

The outputs P_i can be obtained by processing M_i with a 3×3 convolution operation.

3.4. Loss function

Binary Cross-Entropy (BCE) loss is a widely used loss function in camouflaged object detection. However, BCE evaluates the loss of each pixel independently and lacks a global perspective. Wei et al. [52] proposed a hybrid loss combining Weighted Binary Cross-Entropy (wBCE) and Weighted Intersection over Union (wIoU) losses. The loss output is represented as Eq.14:

$$L = L_{wBCE} + L_{wIoU} \quad (14)$$

We employ this hybrid loss to supervise the four outputs of the model, the total training loss for the proposed model can be represented as Eq.15:

$$L_{total} = \sum_{i=1}^4 L(P_i, G) \quad (15)$$

where P_i ($i \in \{1, 2, 3, 4\}$) represents the i -th predicted camouflaged map. In the weakly supervised object detection experiments, G represents M in Eq.1 and the mask processed by RPS. In the fully supervised object detection experiments, G represents the ground truth. P_1 is the final prediction.

4. Experiments

In this section, we introduce the dataset, evaluation metrics and experimental details. We compared weakly supervised and fully supervised COD methods using three commonly used COD datasets. To further demonstrate the general performance of the proposed method, we also tested in SOD with bounding-box supervision on four commonly used SOD datasets. Ablation experiments were conducted on the proposed strategy and individual components of MGNet to verify their effectiveness.

4.1. Datasets and evaluation metrics

4.1.1. Datasets

We evaluated our method on three commonly used datasets, including CAMO dataset [26], COD10K dataset [8], and NC4K dataset [37]. The CAMO dataset consists of 1,000 training images and 250 testing images. The COD10K dataset is the largest camouflaged object dataset with 3,040 images for training and 2,026 images for testing. The NC4K dataset primarily consists of natural images, with its 4,121 images exclusively designated for use as the test set.

In camouflaged object detection task, there are few weakly supervised methods based on bounding-boxes. To

verify the effectiveness of the proposed bounding-box based object detection method, we conducted experiments on SOD. We evaluated our method on four commonly used datasets, including the DUTS-TR dataset [46], the ECSSD dataset [56], the DUT-OMRON dataset [58] and the HKU-IS dataset [27]. DUTS-TR dataset contains 10,553 images. The ECSSD dataset consists of 1,000 images. The HKU-IS dataset contains 4,447 images. The DUT-OMRON dataset contains 5,168 images, and the scenes in this dataset are complex. The DUTS-TE dataset contains 5,019 test images, which contain important scenes for SOD.

To ensure experimental fairness in COD, we used the same dataset partitioning method as existing models [65]. Specifically, 1,000 images from the CAMO dataset and 3,040 images from the COD10K dataset were allocated to the training set, while the remaining 250 images from the CAMO dataset, 2,026 images from the COD10K dataset, and the entire NC4K dataset served as the test set. For SOD, we followed established practices [32], using the DUTS-TR dataset for training and the ECSSD, DUT-OMRON, and HKU-IS datasets for testing.

4.1.2. Evaluation metrics

To comprehensively compare our methods with competing COD methods, we chose four commonly used metrics, including the structural measure (S_α), the adaptive F-measure (F_β), the mean absolute error (\mathcal{M}) and the mean E-measure (E_ϕ). S_α is used to assess the structural similarity between the predicted map and the ground truth. F takes into account both precision and recall. \mathcal{M} represents the average value of the absolute error between the predicted value and the true value. E is employed to assess segmentation results at both the pixel and image levels. Larger values of S_α , F_β , E_ϕ and smaller values of \mathcal{M} indicate better segmentation performance.

To comprehensively compare our methods with competing SOD methods, we chose two commonly used metrics, including the mean absolute error (\mathcal{M}) and the maximum F-measure (F_β^m). Larger values of F_β^m and smaller values of \mathcal{M} indicate better segmentation performance.

4.2. Implementation details

Our proposed BoxSAM and MGNet are implemented based on PyTorch. For SAM, we adopt the ViT-H SAM model [25] to generate segmentation initial pseudo-labels. For MGNet, the backbone (i.e., PVTv2_B2 [50], PVTv2_B4 [50] or Res2Net50 [13]) is initialized with the parameters pre-trained on ImageNet large-scale dataset. In the weakly supervised training phase, the backbone employed is PVTv2_B2, and the model is supervised by processed pseudo-labels during the training process. In contrast, during the fully supervised training phase, the model is supervised by ground truth labels. Apart from this, all other configurations of MGNet remain consistent. The input images are resized to 480×480 . AdamW with an initial learning rate of $1e-4$ is used as the optimizer, and a weight decay of 0.1 is used in the network training. The learning rate decays

Table 1

Quantitative comparison with point supervision, scribble supervision and bounding-box supervision on COD. The best results are highlighted in **Bold**.

Model	Pub/Year	Supervision	CAMO-Test				COD10K-Test				NC4K			
			$S_{\alpha} \uparrow$	$F_{\beta} \uparrow$	$\mathcal{M} \downarrow$	$E_{\phi} \uparrow$	$S_{\alpha} \uparrow$	$F_{\beta} \uparrow$	$\mathcal{M} \downarrow$	$E_{\phi} \uparrow$	$S_{\alpha} \uparrow$	$F_{\beta} \uparrow$	$\mathcal{M} \downarrow$	$E_{\phi} \uparrow$
WSSA [66]	CVPR ₂₀	Point	0.649	0.607	0.148	0.652	0.642	0.509	0.087	0.733	0.743	0.688	0.104	0.756
SCWS [63]	AAAI ₂₁	Point	0.687	0.624	0.142	0.672	0.738	0.593	0.082	0.777	0.754	0.695	0.098	0.767
TEL [29]	CVPR ₂₂	Point	0.645	0.662	0.133	0.674	0.727	0.623	0.063	0.803	0.766	0.725	0.085	0.795
SCOD [16]	AAAI ₂₃	Point	0.663	0.629	0.137	0.688	0.711	0.607	0.060	0.802	0.758	0.744	0.080	0.796
SAM [25]	ICCV ₂₃	Point	0.677	0.649	0.123	0.693	0.765	0.694	0.069	0.796	0.776	0.728	0.082	0.786
WS-SAM [14]	NeurIPS ₂₃	Point	0.718	0.703	0.102	0.757	0.790	0.698	0.039	0.856	0.813	0.801	0.057	0.859
WSSA [66]	CVPR ₂₀	Scribble	0.696	0.615	0.118	0.786	0.684	0.536	0.071	0.770	0.761	0.657	0.091	0.779
SCWS [63]	AAAI ₂₁	Scribble	0.713	0.658	0.102	0.795	0.710	0.602	0.055	0.805	0.784	0.723	0.073	0.814
TEL [29]	CVPR ₂₂	Scribble	0.717	0.681	0.104	0.797	0.724	0.633	0.057	0.826	0.782	0.754	0.075	0.832
SCOD [16]	AAAI ₂₃	Scribble	0.735	0.709	0.092	0.815	0.733	0.637	0.049	0.832	0.779	0.751	0.064	0.853
SAM [25]	ICCV ₂₃	Scribble	0.731	0.682	0.105	0.774	0.772	0.695	0.046	0.828	0.763	0.747	0.071	0.832
WS-SAM [14]	NeurIPS ₂₃	Scribble	0.759	0.742	0.092	0.818	0.803	0.719	0.038	0.878	0.829	0.802	0.052	0.886
SAM-COD [4]	ECCV ₂₄	Bounding-box	0.837	-	0.062	0.901	0.842	-	0.028	0.914	0.867	-	0.037	0.923
BoxSAM-P (Ours)		Point	0.745	0.757	0.102	0.749	0.808	0.756	0.042	0.851	0.810	0.814	0.069	0.823
BoxSAM-S (Ours)		Scribble	0.830	0.789	0.084	0.860	0.836	0.749	0.044	0.883	0.860	0.825	0.052	0.894
BoxSAM (Ours)		Bounding-box	0.859	0.842	0.057	0.908	0.857	0.789	0.027	0.919	0.877	0.854	0.037	0.925

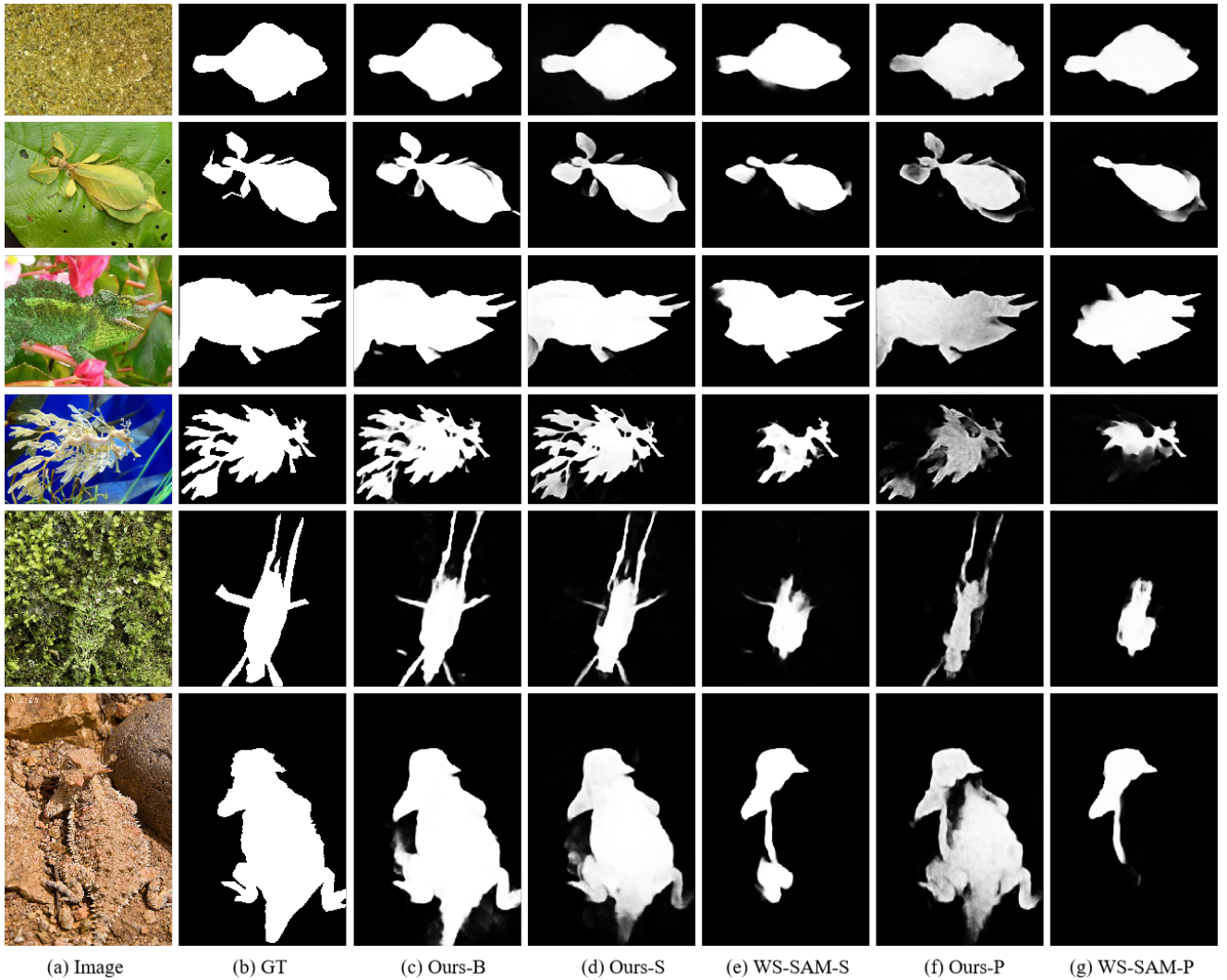


Figure 9: Qualitative comparison with WSCOD methods. (a) RGB images. (b) Ground truth. (c)-(g) The detection results obtained by (c) Our method based on bounding-box supervision, (d) Our method based on scribble supervision, (e) WS-SAM [14] based on scribble supervision, (f) Our method based on point supervision, (g) WS-SAM [14] based on point supervision.

Table 2Quantitative comparison with 3 bounding-box supervision methods on SOD. The best results are highlighted in **Bold**.

Model	Pub/Year	ECSSD		HKU-IS		DUT-OMRON		DUTS-TE	
		$F_{\beta}^m \uparrow$	$\mathcal{M} \downarrow$	$F_{\beta}^m \uparrow$	$\mathcal{M} \downarrow$	$F_{\beta}^m \uparrow$	$\mathcal{M} \downarrow$	$F_{\beta}^m \uparrow$	$\mathcal{M} \downarrow$
SBB [34]	TCSVT ₂₁	0.878	0.072	0.869	0.057	0.751	0.075	0.775	0.073
Wang et al. [47]	JOCA ₂₃	0.894	0.062	0.880	0.052	0.791	0.065	0.806	0.062
Liu et al. [32]	ERA ₂₄	0.945	0.035	0.932	0.031	0.793	0.055	0.889	0.036
BoxSAM (Ours)		0.952	0.029	0.933	0.029	0.825	0.048	0.897	0.033

Table 3Quantitative comparison with 7 CNN-based methods and 10 Transformer-based methods on COD. The best results are highlighted in **Bold**.

Model	Pub/Year	Backbone	CAMO-Test				COD10K-Test				NC4K			
			$S_{\alpha} \uparrow$	$F_{\beta} \uparrow$	$\mathcal{M} \downarrow$	$E_{\phi} \uparrow$	$S_{\alpha} \uparrow$	$F_{\beta} \uparrow$	$\mathcal{M} \downarrow$	$E_{\phi} \uparrow$	$S_{\alpha} \uparrow$	$F_{\beta} \uparrow$	$\mathcal{M} \downarrow$	$E_{\phi} \uparrow$
CNN-Based Methods														
SINet [8]	CVPR ₂₀	ResNet50	0.745	0.712	0.092	0.804	0.776	0.667	0.043	0.864	0.808	0.768	0.058	0.871
UGTR [59]	ICCV ₂₁	ResNet50	0.785	0.749	0.086	0.823	0.818	0.671	0.035	0.853	0.839	0.779	0.052	0.874
SINet-V2 [7]	TPAMI ₂₂	Res2Net50	0.822	0.779	0.070	0.882	0.815	0.682	0.037	0.887	0.847	0.792	0.048	0.903
BSANet [73]	AAAI ₂₂	Res2Net50	0.794	0.768	0.079	0.851	0.818	0.723	0.034	0.891	0.841	0.805	0.048	0.897
PFNet+ [38]	SCIS ₂₃	ResNet50	0.791	0.764	0.080	0.850	0.806	0.698	0.037	0.884	-	-	-	-
MRR-Net [57]	TNNLS ₂₃	Res2Net50	0.826	0.793	0.070	0.880	0.835	0.726	0.032	0.901	0.857	0.807	0.044	0.906
CamoFocus [24]	WACV ₂₄	ResNet50	0.812	0.794	0.071	-	0.830	0.749	0.033	-	0.847	0.812	0.043	-
MGNet-R (Ours)		Res2Net50	0.828	0.791	0.069	0.879	0.843	0.747	0.030	0.905	0.859	0.818	0.044	0.906
Transformer-Based Methods														
DTINet [36]	ICPR ₂₂	MiT	0.856	0.821	0.050	0.916	0.824	0.702	0.034	0.896	0.863	0.809	0.041	0.917
FSPNet [19]	CVPR ₂₃	ViT	0.856	0.829	0.050	0.899	0.851	0.736	0.026	0.895	0.879	0.826	0.035	0.915
MSCAF-Net [33]	TCSVT ₂₃	PVTv2_B2	0.873	0.848	0.046	0.929	0.865	0.775	0.024	0.927	0.887	0.852	0.032	0.929
DGNet [21]	MIR ₂₃	PVTv2_B2	0.866	0.829	0.051	0.919	0.844	0.743	0.029	0.913	0.875	0.832	0.037	0.925
DCNet [65]	TCSVT ₂₃	PVTv2_B2	0.870	-	0.050	0.922	0.873	-	0.022	0.934	-	-	-	-
HitNet [18]	AAAI ₂₃	PVTv2_B2	0.849	-	0.055	0.906	0.871	-	0.023	0.935	0.875	-	0.037	0.926
FSPNet+ [60]	arXiv ₂₄	ViT	0.858	0.836	0.049	0.908	0.847	0.753	0.026	0.899	0.877	0.836	0.035	0.920
IPNet [51]	EAAI ₂₄	PVTv2_B2	0.864	0.846	0.047	0.924	0.850	0.785	0.026	0.922	-	-	-	-
ICEG [15]	ICLR ₂₄	Swin	0.867	0.855	0.044	0.926	0.857	0.782	0.024	0.930	0.879	0.855	0.034	0.932
CamoFormer-P [62]	TPAMI ₂₄	PVTv2_B4	0.872	0.853	0.046	0.929	0.869	0.794	0.023	0.932	0.892	0.863	0.030	0.939
MGNet (Ours)		PVTv2_B2	0.882	0.859	0.044	0.933	0.878	0.800	0.022	0.934	0.893	0.860	0.032	0.936
MGNet-B4 (Ours)		PVTv2_B4	0.887	0.872	0.041	0.941	0.883	0.807	0.021	0.938	0.896	0.868	0.029	0.942

by a factor of 10 after 50 epochs. If either PVTv2_B2 or Res2Net50 is chosen as the backbone, the batch size is set to 16. If PVTv2_B4 is chosen as the backbone, the batch size is set to 12. The entire model is trained for 100 epochs. The whole model is trained and tested on a single NVIDIA 3090 GPU.

4.3. Comparison with state-of-the-arts

To verify the superiority of our method in the task of WSCOD, we compared with several state-of-the-art methods, including WSSA [66], SCWS [63], TEL [29], SCOD [16], SAM [25], WS-SAM [14] and SAM-COD [4]. The backbone architectures of WSSA, SCWS, TEL, SCOD, SAM, WS-SAM, and SAM-COD are VGG16, ResNet50, ResNet101, ResNet50, ViT-H, ViT-H and ResNet50, and ViT-H and PVT-B4, respectively. In BoxSAM with scribble annotations, we used pixel-level weighted data generated by [14] without any additional screening. In BoxSAM with point annotations, following the previous weakly supervised segmentation method [12], one point was randomly selected from the foreground and one point was randomly selected from the background.

Due to the scarcity of weak supervision based on bounding-boxes in COD, we compared the proposed BoxSAM with methods in salient object detection task, including SBB [34],

the method proposed by Wang et al. [47] and the method proposed by Liu et al. [32].

For fully supervised COD, we conducted a comparison with 17 main camouflaged object detection methods, which included 7 CNN-based COD models (SINet [8], UGTR [59], SINet-V2 [7], BSANet [73], PFNet+ [38], MRR-Net [57], CamoFocus [24]) and 10 Transformer-based COD models (DTINet [36], FSPNet [19], MSCAF-Net [33], DGNet [21], DCNet [65], HitNet [18], FSPNet+ [60], IPNet [51], ICEG [15], CamoFormer-P [62]). All predictions made by the competitors were provided by the authors.

4.3.1. Quantitative evaluation

Table 1 shows the quantitative comparison between BoxSAM and other weakly supervised COD models on public datasets. The results indicate that our model achieves superior performance on multiple evaluation metrics of the three datasets with scribble supervision and bounding-box supervision. In point supervision, BoxSAM improves the S_{α} by 3.8% and 2.3% on the CAMO and COD10K datasets compared with the suboptimal model, respectively. In scribble supervision, compared with the latest WSCOD method WS-SAM [14], S_{α} and F_{β} achieve an average

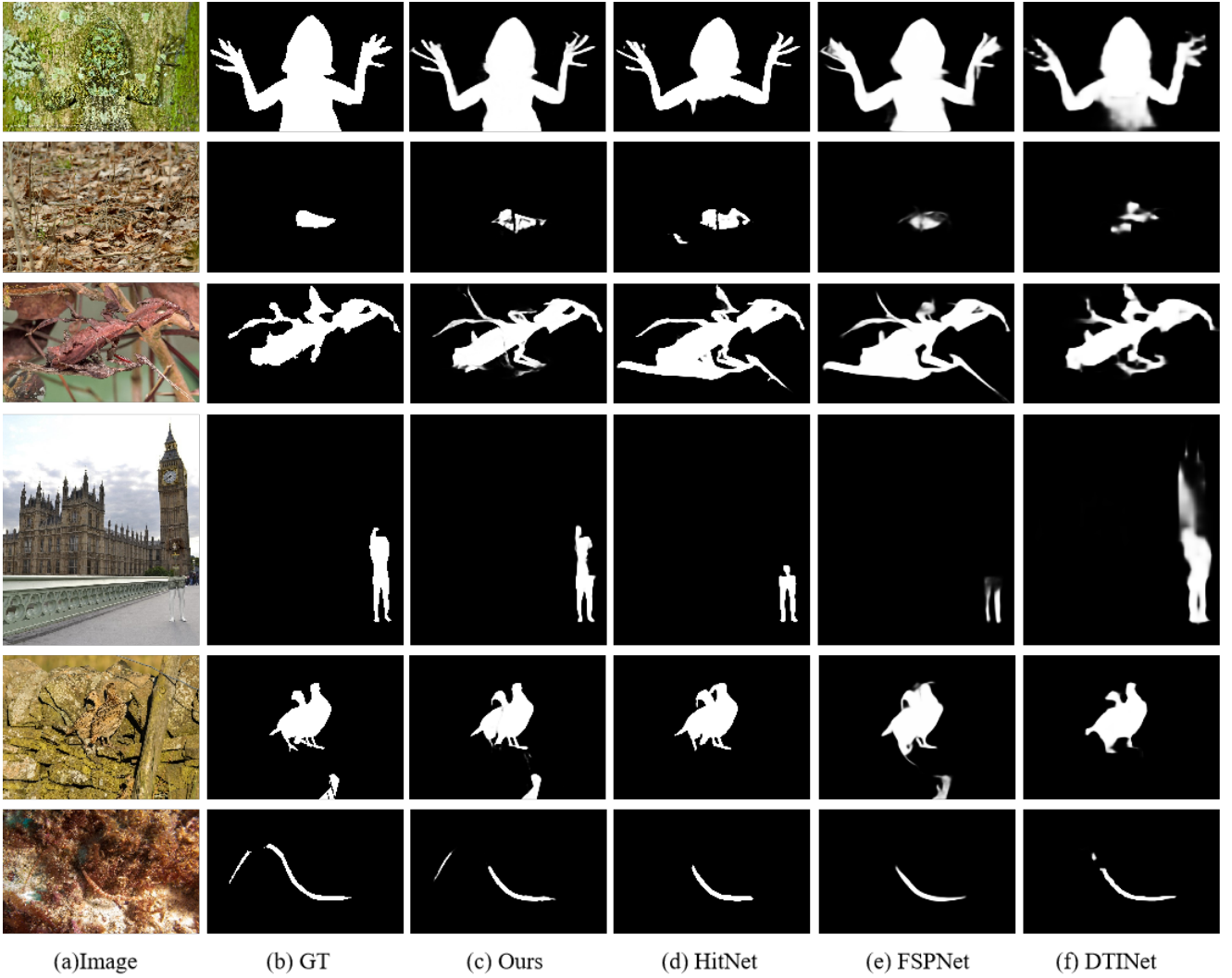


Figure 10: Qualitative comparison with Transformer-based COD methods. (a) RGB images. (b) Ground truth. (c)-(f) The detection results obtained by (c) Our method based on Transformer, (d) HitNet [18], (e) FSPNet [19], (f) DTINet [36].

Table 4

Ablation study of BoxSAM on three datasets. The best results are highlighted in **Bold**.

Model	CAMO-Test				COD10K-Test				NC4K			
	$S_\alpha \uparrow$	$F_\beta \uparrow$	$\mathcal{M} \downarrow$	$E_\phi \uparrow$	$S_\alpha \uparrow$	$F_\beta \uparrow$	$\mathcal{M} \downarrow$	$E_\phi \uparrow$	$S_\alpha \uparrow$	$F_\beta \uparrow$	$\mathcal{M} \downarrow$	$E_\phi \uparrow$
BoxSAM + w/o RPS	0.854	0.835	0.061	0.901	0.858	0.784	0.029	0.918	0.876	0.848	0.038	0.922
MGNet + ADELE [31]	0.853	0.833	0.059	0.905	0.857	0.783	0.028	0.916	0.877	0.849	0.038	0.923
BoxSAM (Ours)	0.859	0.842	0.057	0.908	0.857	0.789	0.027	0.919	0.877	0.854	0.037	0.925

enhancement of 5.7% and 4.5%, respectively. In bounding-box supervision, our proposed method demonstrates a notable improvement in S_α metric, with an increase of 2.6%, compared to the suboptimal method SAM-COD [4] on the CAMO dataset. Table 2 shows the quantitative comparison results of BoxSAM with other weakly supervised SOD models, BoxSAM improves F_β^m by 4.0% on the DUT-OMRON dataset compared to the suboptimal model.

Table 3 shows the quantitative comparison results of MGNet with other CNN and transformer based COD models. The results indicate that our model achieves the best

performance on S_α when using CNN as the backbone, outperforming other models that also use CNN backbones. In models employing PVTv2 as the backbone, on both the CAMO and COD10K datasets, the proposed MGNet demonstrates average improvements of 1.3% and 2.3% in the S_α and F_β metrics, respectively, in comparison to the suboptimal method MSCAF-Net [33]. Moreover, compared to CamoFormer-P [62], which uses PVTv2_B4 as the backbone, our proposed MGNet_B4 achieves improvements of 1.7% and 1.6% in S_α on the CAMO and COD10K datasets, respectively.

Table 5

Ablation study of MGNet on two datasets. CMD: Cascaded Mask Decoder. CEM: Context Enhancement Module. MFAM: Mask-guided Feature Aggregation Module. The best results are highlighted in **Bold**.

No	Backbone	Module			CAMO-Test				COD10K-Test			
		CMD	CEM	MFAM	$S_\alpha \uparrow$	$F_\beta \uparrow$	$\mathcal{M} \downarrow$	$E_\phi \uparrow$	$S_\alpha \uparrow$	$F_\beta \uparrow$	$\mathcal{M} \downarrow$	$E_\phi \uparrow$
#1	PVTv2_B2				0.869	0.838	0.051	0.918	0.866	0.775	0.024	0.930
#2	PVTv2_B2	✓			0.875	0.843	0.048	0.923	0.871	0.778	0.023	0.931
#3	PVTv2_B2		✓		0.871	0.840	0.049	0.922	0.874	0.792	0.023	0.934
#4	PVTv2_B2	✓	✓		0.875	0.845	0.048	0.925	0.876	0.795	0.023	0.934
#5	PVTv2_B2	✓		✓	0.876	0.855	0.046	0.925	0.876	0.803	0.023	0.933
#6	PVTv2_B2		✓	✓	0.877	0.849	0.047	0.928	0.877	0.795	0.022	0.935
#7	PVTv2_B2	✓	✓	✓	0.882	0.859	0.044	0.933	0.878	0.800	0.022	0.934
#8	Res2Net50	✓	✓	✓	0.828	0.791	0.069	0.879	0.843	0.747	0.030	0.905
#9	PVTv2_B4	✓	✓	✓	0.887	0.872	0.041	0.941	0.883	0.807	0.021	0.938

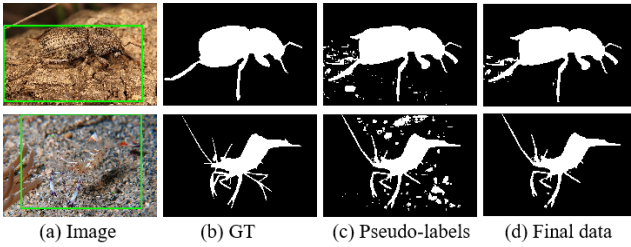


Figure 11: Some examples of masks. (a) RGB images. (b) Ground truth. (c) Some examples of SAM segmentation with bounding-boxes. (d) Some examples of masks after redundancy processing.

4.3.2. Qualitative comparisons

Figure 9 compares the visual quality of WSCOD between our proposed BoxSAM method and WS-SAM using various supervised methods. This qualitative comparison covers various challenging scenarios, including highly intrinsic similarities (rows 1, 2 and 3), complex edges (row 4), and complex backgrounds (rows 5 and 6). Our method, which employs point and scribble supervision, effectively identifies more complete camouflaged objects. This improvement is largely attributed to the design of BoxSAM. Compared to point and scribble supervision, BoxSAM provides clearer edge details when using bounding-box supervision. This improvement is due to the use of the SAM model with bounding-box annotations as prompts.

Figure 10 presents the visualization of prediction results for Transformer-based fully supervised methods. This qualitative comparison covers various challenging scenarios scenes, including highly intrinsic similarities (row 1), tiny objects (rows 2 and 6), complex backgrounds (rows 3 and 5), and indefinable edges (row 4). Most methods struggle to extract edges of camouflaged objects, leading to incomplete segmentation (rows 1, 2, 3 and 4). In contrast, our method achieves complete segmentation of camouflaged objects. Additionally, small or obscured camouflaged objects are often missed (rows 5 and 6). MGNet delivers better prediction masks compared with other competing methods.

4.4. Ablation study

To demonstrate the effectiveness of our proposed modules, we conducted ablation studies on three benchmark datasets. The quantitative results of these studies are presented in Tables 4, 5, 6, 7 and 8.

4.4.1. Effectiveness of RPS

To reduce redundant information in the pseudo-labels generated by SAM, we develop the Redundancy Processing Strategy (RPS). To verify its effectiveness, we removed the RPS and used the pseudo-labels generated by SAM directly as the training set for the MGNet model. The results indicate that the performance of our proposed BoxSAM method decreases without the RPS strategy, as shown in Table 4. For instance, the F_β drops by an average of 0.7%. This demonstrates that the RPS enhances the quality of training labels for MGNet, thereby improving segmentation performance. Additionally, we compared RPS with ADELE [31], and the results demonstrate that our method achieves superior segmentation performance. This is primarily because our method is specifically designed for pseudo-labels generated by SAM for camouflaged objects.

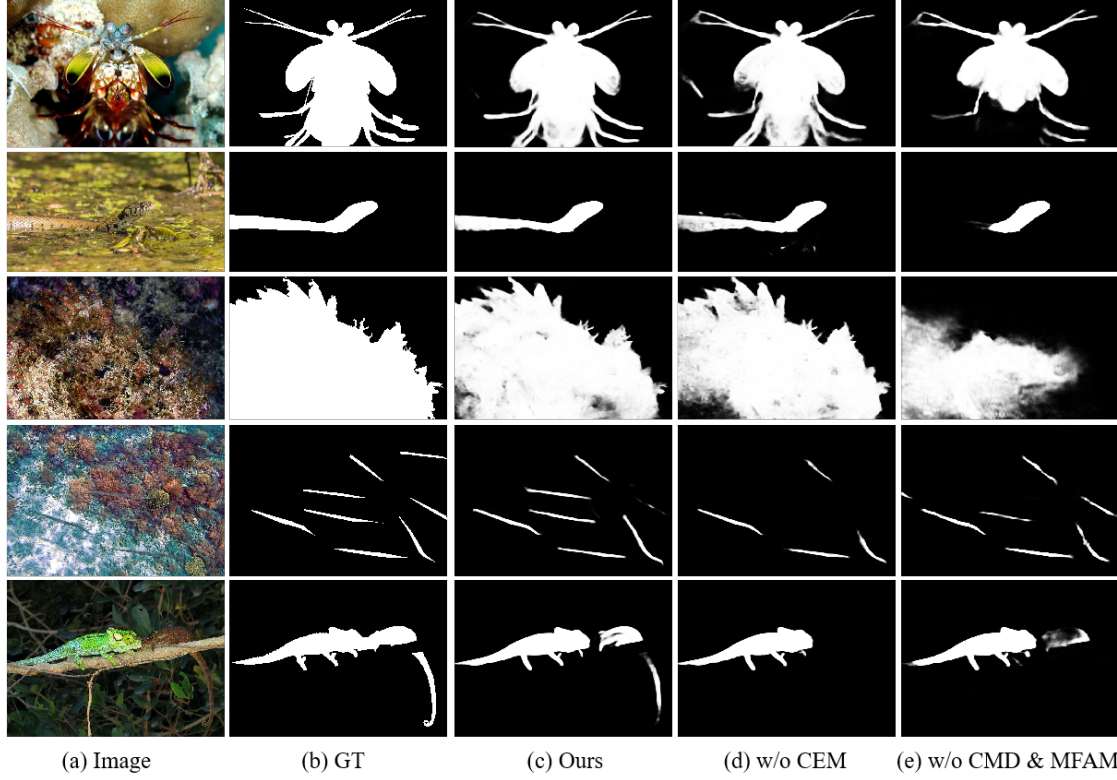
To enhance readability, we provide some demonstrations in Figure 11. As shown in (c), the initial labels generated by SAM using bounding-boxes as prompts contain redundant information. Specifically, due to the considerable high similarity between objects and their surroundings, certain areas of the background are incorrectly identified as camouflaged objects. This incorrect identification adversely affects the model's accuracy and training effectiveness. In contrast, (d) demonstrates a significant improvement in the quality of the training labels after redundancy processing. By eliminating redundant information, this processing improves the quality of the training labels, enabling the MGNet to more accurately identify and segment camouflaged objects.

4.4.2. Effectiveness of MGNet

To validate the effectiveness of MGNet in BoxSAM, we replaced MGNet in BoxSAM with other COD models for comparison. The models included SINet [8], SINet-V2 [7], HitNet [18], and MSCAF-Net [33]. The results are shown in Table 6. For instance, on the CAMO and COD10K

Table 6Quantitative comparison with other models on BoxSAM. The best results are highlighted in **Bold**.

Model	Backbone	CAMO-Test				COD10K-Test				NC4K			
		$S_\alpha \uparrow$	$F_\beta \uparrow$	$M \downarrow$	$E_\phi \uparrow$	$S_\alpha \uparrow$	$F_\beta \uparrow$	$M \downarrow$	$E_\phi \uparrow$	$S_\alpha \uparrow$	$F_\beta \uparrow$	$M \downarrow$	$E_\phi \uparrow$
BoxSAM(MGNet→SINet [8])	ResNet50	0.728	0.704	0.104	0.753	0.763	0.621	0.048	0.814	0.803	0.755	0.063	0.842
BoxSAM(MGNet→SINet-V2[7])	Res2Net50	0.799	0.766	0.084	0.852	0.802	0.680	0.041	0.874	0.836	0.788	0.052	0.893
BoxSAM(MGNet→HitNet [18])	PVTv2_B2	0.823	0.805	0.068	0.882	0.841	0.777	0.031	0.906	0.851	0.824	0.046	0.902
BoxSAM(MGNet→MSCAF-Net [33])	PVTv2_B2	0.841	0.821	0.062	0.897	0.845	0.763	0.030	0.912	0.873	0.845	0.038	0.923
BoxSAM(Ours)	Res2Net50	0.806	0.786	0.077	0.856	0.824	0.735	0.034	0.890	0.844	0.813	0.049	0.893
BoxSAM (Ours)	PVTv2_B2	0.859	0.842	0.057	0.908	0.857	0.789	0.027	0.919	0.877	0.854	0.037	0.925

**Figure 12:** Visual verification of the effectiveness of the proposed components. (a) RGB images. (b) Ground truth. (c)-(e) The detection results obtained by (c) Our method (MGNet), (d) MGNet without CEM, (e) MGNet without CMD and MFAM.

datasets, the S_α improves by an average of 1.8% compared to the suboptimal MSCAF-Net, and the F_β improves by an average of 3.0% compared to the suboptimal MSCAF-Net. The segmentation results in BoxSAM are better when using MGNet.

4.4.3. Effectiveness of CMD

We conducted ablation experiments to assess the effectiveness of the Cascaded Mask Decoder (CMD). The results of these experiments are illustrated in Tables 5 and 7.

We contrasted the network with the cascade operation and CBAM [53] removed (denoted as #6) against the network with CMD included (denoted as #7), as shown in Table 5. The removal of CMD results in performance drop, indicating that it contributes to improving detection performance.

In addition, we output the final prediction using the CMD (denoted as #2), as shown in Table 5. The results demonstrate that our designed module improves upon the baseline metrics, indicating that the proposed module can

Table 7Ablation study of Cascaded Mask Decoder on three datasets. The best result are highlighted in **Bold**.

CEM	CAMO-Test				COD10K				NC4K			
	$S_\alpha \uparrow$	$F_\beta \uparrow$	$M \downarrow$	$E_\phi \uparrow$	$S_\alpha \uparrow$	$F_\beta \uparrow$	$M \downarrow$	$E_\phi \uparrow$	$S_\alpha \uparrow$	$F_\beta \uparrow$	$M \downarrow$	$E_\phi \uparrow$
MGNet + w/o Cascade	0.877	0.852	0.046	0.931	0.876	0.790	0.023	0.934	0.890	0.858	0.032	0.935
MGNet + w/o CBAM	0.879	0.856	0.046	0.929	0.878	0.799	0.022	0.936	0.891	0.859	0.032	0.935
MGNet (Ours)	0.882	0.859	0.044	0.933	0.878	0.800	0.022	0.934	0.893	0.860	0.032	0.936

Table 8Ablation study of Context Enhancement Module on three datasets. The best results are highlighted in **Bold**.

CEM	CAMO-Test				COD10K				NC4K			
	$S_\alpha \uparrow$	$F_\beta \uparrow$	$\mathcal{M} \downarrow$	$E_\phi \uparrow$	$S_\alpha \uparrow$	$F_\beta \uparrow$	$\mathcal{M} \downarrow$	$E_\phi \uparrow$	$S_\alpha \uparrow$	$F_\beta \uparrow$	$\mathcal{M} \downarrow$	$E_\phi \uparrow$
CEM \rightarrow ASPP	0.879	0.852	0.046	0.928	0.877	0.796	0.023	0.935	0.892	0.856	0.032	0.935
MGNet + w/o Conv	0.878	0.856	0.045	0.926	0.876	0.799	0.023	0.935	0.891	0.861	0.033	0.933
MGNet + w/o BA	0.880	0.857	0.046	0.929	0.877	0.795	0.023	0.933	0.892	0.858	0.032	0.937
MGNet (Ours)	0.882	0.859	0.044	0.933	0.878	0.800	0.022	0.934	0.893	0.860	0.032	0.936

Table 9Ablation study of loss on three datasets. The best result are highlighted in **Bold**.

Loss	CAMO-Test				COD10K				NC4K			
	$S_\alpha \uparrow$	$F_\beta \uparrow$	$\mathcal{M} \downarrow$	$E_\phi \uparrow$	$S_\alpha \uparrow$	$F_\beta \uparrow$	$\mathcal{M} \downarrow$	$E_\phi \uparrow$	$S_\alpha \uparrow$	$F_\beta \uparrow$	$\mathcal{M} \downarrow$	$E_\phi \uparrow$
L_{NC} [67]	0.845	0.836	0.060	0.903	0.854	0.792	0.029	0.917	0.871	0.853	0.038	0.923
BoxSAM(Ours)	0.859	0.842	0.057	0.908	0.857	0.789	0.027	0.919	0.877	0.854	0.037	0.925
L_{NC} [67]	0.870	0.865	0.045	0.932	0.872	0.813	0.022	0.930	0.885	0.867	0.032	0.932
MGNet (Ours)	0.882	0.859	0.044	0.933	0.878	0.800	0.022	0.934	0.893	0.860	0.032	0.936

generate more accurate initial masks and effectively guide the subsequent segmentation process.

We further investigated this by removing the cascade operation and retaining the lowest-level features, as shown in the first row of Table 7. This leads to a decline in segmentation performance, demonstrating that the cascade operation provides a more accurate mask for guiding subsequent generation. Additionally, we utilize CBAM to capture the details of camouflaged objects from different dimensions of the low-level feature map. To assess its effectiveness, we also examined the performance impact of removing CBAM from MGNet. As shown in the second row of Table 7, the removal of CBAM causes a decline in performance.

4.4.4. Effectiveness of CEM

To expand the receptive field and introduce rich context information, we propose the Context Enhancement Module (CEM). To evaluate the effectiveness of the CEM, we removed it (denoted as #5) and the output of the encoder was directly input into the Mask-guided Feature Aggregation Module (MFAM) for aggregation, as shown in Table 5. By comparing the results in the #5 and #7 of Table 5, the removal of the CEM has resulted in performance drop. The quantitative comparison demonstrates that CEM can expand the receptive field and introduce rich contextual information. The efficacy of our CEM is visually demonstrated in Figure 12, as shown in (c) and (d), methods with the CEM can reduce the missing detection.

In addition, we incorporated the CEM (denoted as #3) into the baseline model (denoted as #1) to validate its effectiveness. Comparing #3 with the baseline, we observe improved performance in all evaluation metrics. Notably, the F_β shows an improvement of 2.1% on the COD10K dataset. These experimental results demonstrate that our CEM significantly contributes to more accurate detection of camouflaged objects within the network.

Furthermore, we replaced CEM with ASPP [5], as shown in the first row of Table 8. The experimental results

demonstrate that the CEM designed by us exhibits superior performance. We further investigated this by removing the dilated convolution, which leads to decreased segmentation performance, as shown in the second row of Table 8. Additionally, we examined the impact of the BA [18] on segmentation performance. As indicated in the third row of Table 8, the removal of the BA resulted in performance degradation, hindering the accurate segmentation of detailed information.

4.4.5. Effectiveness of MFAM

In order to effectively aggregate features, we design the Mask-guided Feature Aggregation Module (MFAM). To evaluate the effectiveness of the MFAM, we replaced it (denoted as #4) with element-wise multiplication, convolutional layers and concatenation, as shown in Table 5. By comparing the results in the #4 and #7 of Table 5, we can observe that the removal of MFAM can cause a performance drop on CAMO and COD10K datasets. This indicates that MFAM plays a positive role in the COD task.

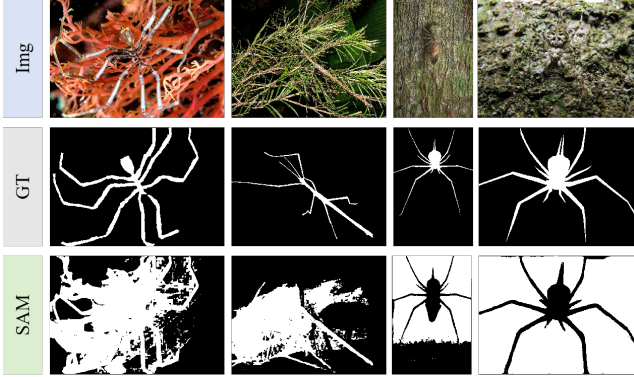
We further investigated the detection performance without CMD and MFAM (denoted as #3), as shown in Table 5. By comparing the results in the #3 and #7 of Table 5, there is performance drop when removing CMD and MFAM from the proposed MGNet. For instance, there are S_α and F_β drop of 1.3% and 2.3% on CAMO dataset, respectively. These findings suggest that feature aggregation based on mask guidance significantly enhances segmentation performance. The efficacy of our CMD and MFAM is demonstrated visually in Figure 12, as shown in (c) and (e), methods with CMD and MFAM can generate the predictions with clear edges.

4.4.6. Effectiveness of PVTv2

To effectively extract features, we choose the Pyramid Vision Transformer (PVT) [49] as our feature extraction module. To evaluate the effectiveness of the PVTv2 as the backbone, we replaced PVTv2_B2 [50] with Res2Net50 [13], which is pre-trained on the ImageNet large-scale

Table 10Quantitative comparison with 3 polyp segmentation methods and 2 COD methods. The best results are highlighted in **Bold**.

Model	Pub/Year	CVC-ColonDB					CVC-ClinicDB				
		$mDice \uparrow$	$mIoU \uparrow$	$S_\alpha \uparrow$	$\mathcal{M} \downarrow$	$E_\phi \uparrow$	$mDice \uparrow$	$mIoU \uparrow$	$S_\alpha \uparrow$	$\mathcal{M} \downarrow$	$E_\phi \uparrow$
PraNet [10]	MICCAI ₂₀	0.703	0.634	0.815	0.037	0.835	0.916	0.870	0.946	0.007	0.973
SSFormer [42]	MMSP ₂₂	0.756	0.683	0.841	0.034	0.875	0.908	0.861	0.938	0.009	0.965
SINet-V2 [7]	TPAMI ₂₂	0.746	0.668	0.840	0.035	0.871	0.903	0.852	0.935	0.012	0.959
HitNet [18]	AAAI ₂₃	0.752	0.669	0.833	0.035	0.874	0.908	0.855	0.936	0.010	0.964
PVT-CASCADE [41]	WACV ₂₃	0.801	0.725	0.862	0.029	0.903	0.940	0.895	0.952	0.006	0.983
MGNet (Ours)		0.807	0.731	0.871	0.031	0.907	0.941	0.895	0.955	0.006	0.986

**Figure 13:** Failure cases of SAM segmentation results using bounding-box prompts.

dataset. By comparing the results in the #7 and #8 of Table 5, we can observe that Transformer-based model shows more obvious advantages compared with CNN-based model. Specifically, compared to methods using Res2Net50 as the backbone, S_α , F_β , and E_ϕ achieved average improvements of 5.3%, 7.8%, and 4.7%, respectively, on the CAMO and COD10K datasets.

Furthermore, we employed PVTv2_B4 as the backbone for our model, as shown in #9 of Table 5. We can observe that PVTv2_B4 achieves better segmentation performance compared to PVTv2_B2. However, it is noteworthy that PVTv2_B4 has a larger number of parameters than PVTv2_B2 [50]. Specifically, with the replacement of the feature extractor, the parameter count of MGNet with PVTv2_B4 as the backbone reaches 63.67M, which is more than double that of MGNet with PVTv2_B2 as the backbone.

4.4.7. Effectiveness of Loss

We evaluated the impact of the adopted loss function, as defined in Eq. 15, and the noise correction loss (L_{NC}) [67] on the experimental results. Following the settings in [67], we applied L_{NC} as the loss function for both weakly supervised COD and fully supervised COD, as shown in Table 9. The results show that L_{NC} improves the F_β metric, as it is designed to enhance the model's robustness to noisy labels [67]. However, Eq. 15 demonstrates superior performance across the majority of the evaluated metrics, as it accounts for pixel-wise differences more effectively.

Table 11

Comparison of model parameters (Params) and FLOPs.

Model	MGNet (Ours)	DCNet	HitNet	MSCAF-Net
Params	26.48 M	54.43 M	25.73 M	29.70 M
FLOPs	31.81 G	94.74 G	33.86 G	30.04 G

4.4.8. Efficiency analysis

To comprehensively evaluate our model, we investigated and compared our proposed MGNet with competing methods in terms of the floating point operations (FLOPs) and the number of parameters (Params) with three other COD models, as shown in Table 11. It can be seen that our proposed MGNet has lower computational complexity and fewer parameters.

4.5. Limitation

Although the BoxSAM proposed in this paper demonstrates positive effects in various experiments, the segmentation results generated by SAM with bounding-boxes as prompts exhibit failures, such as segmentation errors (columns 1 and 2) and failure to identify camouflaged objects (columns 3 and 4), as shown in Figure 13. Several studies [22, 45, 23] have also highlighted the limitations of SAM in COD. Unfortunately, the approach outlined in this paper is not fully effective in addressing these challenges. Further research needs to focus on improving the accuracy of the generated initial pseudo-labels, such as by effectively combining multiple annotation methods as prompts for large models.

4.6. COD-related applications

In this study, we further validated the effectiveness of our proposed MGNet on two COD-related tasks. The application of polyp segmentation is detailed in Section 4.6.1, while the application of defect detection is discussed in Section 4.6.2.

4.6.1. Polyp segmentation

Polyp segmentation is critical for the precise identification of early polyps, which plays a vital role in the clinical prevention of rectal cancer [10]. To validate the effectiveness of our method in polyp segmentation, we retrained MGNet following [10]. We used 900 images from Kvasir [20] and 550 images from CVC-ClinicDB [2] for the training set, while the remaining images from CVC-ClinicDB and CVC-ColonDB [44] were used for testing. The evaluation

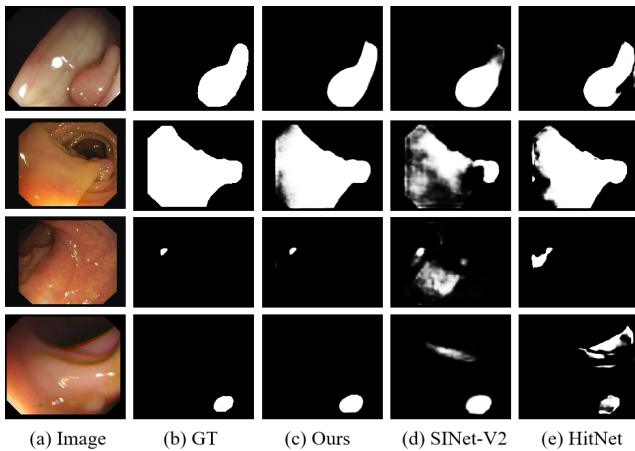


Figure 14: Qualitative comparison on CVC-ClinicDB dataset [2] and CVC-ColonDB [44] dataset. (a) RGB images. (b) Ground truth. (c)-(e) The detection results obtained by (c) Our method, (d) SINet-V2[7], (e) HitNet[18].

metrics include $mDice$, $mIoU$, S_α , \mathcal{M} , and E_ϕ . Among these metrics, $Dice$ and IoU are region-level similarity measures that primarily assess the internal consistency of object segmentation. Larger values of $mDice$, $mIoU$, S_α , E_ϕ and smaller values of \mathcal{M} indicate better segmentation performance.

We compared the performance of MGNet with three polyp segmentation methods, PraNet [10], SSFormer [42], and PVT-CASCADE [41], and with two COD methods, SINet-V2 [7] and HitNet [18]. Some results were sourced from the original papers, while others were obtained by training and testing on equipment with the same configuration as MGNet. The quantitative results are presented in Table 10. MGNet outperforms PraNet [10], SSFormer [42], SINet-V2 [7], and HitNet [18] in terms of performance on CVC-ClinicDB. MGNet improves $mDice$, $mIoU$ and S_α by 0.7%, 0.8% and 1.0%, respectively, in CVC-ColonDB compared to the suboptimal model PVT-CASCADE [41]. The visualization results in Figure 14 illustrate the segmentation performance of MGNet in comparison to SINet-V2 [7] and HitNet [18]. This qualitative comparison covers large polyps (rows 1 and 2) and tiny polyps (rows 3 and 4). As shown in Figure 14, our proposed MGNet can identify polyps well and perform better than competing methods in these challenging cases.

4.6.2. Defect detection

Defect detection is the process of identifying and locating defects or anomalies in products or materials through various techniques and methods, with the aim of ensuring that products meet quality standards and can be used safely. To validate our method's effectiveness in defect detection, we retrained MGNet on the CDS2K dataset [9], using 80% of the dataset for training and the remaining 20% for testing. The evaluation metrics include S_α , F_β , \mathcal{M} and E_ϕ .

We compared the performance of MGNet with three COD methods, SINet [8], SINet-V2 [7] and MSCAF-Net

Table 12

Quantitative comparison with 3 COD methods on the CDS2K dataset. The best results are highlighted in **Bold**.

Model	Pub/Year	CDS2K			
		$S_\alpha \uparrow$	$F_\beta \uparrow$	$\mathcal{M} \downarrow$	$E_\phi \uparrow$
SINet [42]	CVPR ₂₀	0.623	0.421	0.061	0.749
SINet-V2 [7]	TPAMI ₂₂	0.832	0.671	0.010	0.906
MSCAF-Net [18]	TCSVT ₂₃	0.865	0.719	0.009	0.933
MGNet (Ours)		0.877	0.772	0.009	0.944

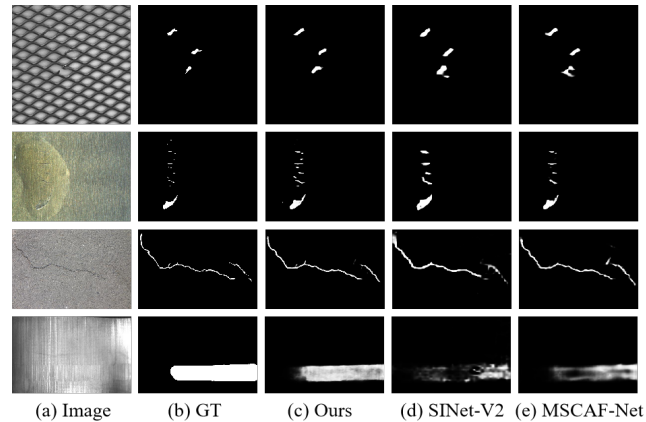


Figure 15: Qualitative comparison on CDS2K dataset [9]. (a) RGB images. (b) Ground truth. (c)-(e) The detection results obtained by (c) Our method, (d) SINet-V2 [7], (e) MSCAF-Net [33].

[33]. The results were obtained by training and testing on equipment with the same configuration as MGNet. The quantitative results are presented in Table 12. MGNet improves S_α , F_β , and E_ϕ by 1.4%, 7.3%, and 1.2%, respectively, compared to the suboptimal model MSCAF-Net [33]. The visualization results in Figure 15 illustrate the segmentation performance of MGNet in comparison to SINet-V2 [7] and MSCAF-Net [33]. This qualitative comparison covers texture-grid (row 1), steel surface (row 2), road surface (row 3) and magnetic tile surface (row 4). As shown in Figure 15, our proposed MGNet can effectively identify defects across different materials and outperforms competing methods in these challenging cases.

5. Discussions and conclusion

In this paper, we propose a new WSCOD method characterized by two key components. The first component generates pseudo-labels by using the bounding-boxes of camouflaged objects as prompts for the SAM model. The second component involves redundant processing strategy that provides high-quality pixel-level pseudo-labels for training our designed Mask-guided Network (MGNet). MGNet includes a Cascaded Mask Decoder (CMD) to progressively integrate information from each layer to produce masks. The Context Enhancement Module (CEM) supplements the missing details of features and avoids the missing detection. Finally,

the Mask-guided Feature Aggregation Module (MFAM) aggregates features across different levels guided by masks to generate predictions with clear object edges.

BoxSAM is evaluated on three widely used COD datasets, demonstrating superior performance compared to current state-of-the-art WSCOD methods. It also achieves state-of-the-art results in weakly supervised SOD using bounding-box supervision. MGNet performs effectively in both COD and other COD-related applications, such as polyp segmentation and defect detection. However, BoxSAM still exhibits some limitations in segmenting camouflaged objects. Further research needs to focus on improving the accuracy of the generated initial pseudo-labels, such as by effectively combining multiple annotation methods as prompts for large models.

References

- [1] Bearman, A., Russakovsky, O., Ferrari, V., Fei-Fei, L., 2016. What's the point: Semantic segmentation with point supervision, in: European conference on computer vision, Springer. pp. 549–565.
- [2] Bernal, J., Sánchez, F.J., Fernández-Esparrach, G., Gil, D., Rodríguez, C., Vilariño, F., 2015. Wm-dova maps for accurate polyp highlighting in colonoscopy: Validation vs. saliency maps from physicians. *Computerized medical imaging and graphics* 43, 99–111.
- [3] Chen, C., Miao, J., Wu, D., Zhong, A., Yan, Z., Kim, S., Hu, J., Liu, Z., Sun, L., Li, X., et al., 2024a. Ma-sam: Modality-agnostic sam adaptation for 3d medical image segmentation. *Medical Image Analysis*, 103310.
- [4] Chen, H., Wei, P., Guo, G., Gao, S., 2024b. Sam-cod: Sam-guided unified framework for weakly-supervised camouflaged object detection. *European Conference on Computer Vision*.
- [5] Chen, L.C., Papandreou, G., Kokkinos, I., Murphy, K., Yuille, A.L., 2017. Deeplab: Semantic image segmentation with deep convolutional nets, atrous convolution, and fully connected crfs. *IEEE transactions on pattern analysis and machine intelligence* 40, 834–848.
- [6] Chen, Z., Gao, R., Xiang, T.Z., Lin, F., 2023. Diffusion model for camouflaged object detection, in: *ECAI 2023*. IOS Press, pp. 445–452.
- [7] Fan, D.P., Ji, G.P., Cheng, M.M., Shao, L., 2021. Concealed object detection. *IEEE transactions on pattern analysis and machine intelligence* 44, 6024–6042.
- [8] Fan, D.P., Ji, G.P., Sun, G., Cheng, M.M., Shen, J., Shao, L., 2020a. Camouflaged object detection, in: *Proceedings of the IEEE/CVF conference on computer vision and pattern recognition*, pp. 2777–2787.
- [9] Fan, D.P., Ji, G.P., Xu, P., Cheng, M.M., Sakaridis, C., Van Gool, L., 2023. Advances in deep concealed scene understanding. *Visual Intelligence* 1, 16.
- [10] Fan, D.P., Ji, G.P., Zhou, T., Chen, G., Fu, H., Shen, J., Shao, L., 2020b. Pranet: Parallel reverse attention network for polyp segmentation, in: *International conference on medical image computing and computer-assisted intervention*, Springer. pp. 263–273.
- [11] Fuentes, A., Yoon, S., Kim, S.C., Park, D.S., 2017. A robust deep-learning-based detector for real-time tomato plant diseases and pests recognition. *Sensors* 17, 2022.
- [12] Gao, S., Xing, H., Zhang, W., Wang, Y., Guo, Q., Zhang, W., 2022. Weakly supervised video salient object detection via point supervision, in: *Proceedings of the 30th ACM International Conference on Multimedia*, pp. 3656–3665.
- [13] Gao, S.H., Cheng, M.M., Zhao, K., Zhang, X.Y., Yang, M.H., Torr, P., 2019. Res2net: A new multi-scale backbone architecture. *IEEE transactions on pattern analysis and machine intelligence* 43, 652–662.
- [14] He, C., Li, K., Zhang, Y., Xu, G., Tang, L., Zhang, Y., Guo, Z., Li, X., 2023a. Weakly-supervised concealed object segmentation with sam-based pseudo labeling and multi-scale feature grouping. *Advances in Neural Information Processing Systems* 36.
- [15] He, C., Li, K., Zhang, Y., Zhang, Y., Guo, Z., Li, X., Danelljan, M., Yu, F., 2024. Strategic preys make acute predators: Enhancing camouflaged object detectors by generating camouflaged objects, in: *International Conference on Learning Representations*.
- [16] He, R., Dong, Q., Lin, J., Lau, R.W., 2023b. Weakly-supervised camouflaged object detection with scribble annotations, in: *Proceedings of the AAAI Conference on Artificial Intelligence*, pp. 781–789.
- [17] Hou, J.Y.H.W., Li, J., 2011. Detection of the mobile object with camouflage color under dynamic background based on optical flow. *Procedia Engineering* 15, 2201–2205.
- [18] Hu, X., Wang, S., Qin, X., Dai, H., Ren, W., Luo, D., Tai, Y., Shao, L., 2023. High-resolution iterative feedback network for camouflaged object detection, in: *Proceedings of the AAAI Conference on Artificial Intelligence*, pp. 881–889.
- [19] Huang, Z., Dai, H., Xiang, T.Z., Wang, S., Chen, H.X., Qin, J., Xiong, H., 2023. Feature shrinkage pyramid for camouflaged object detection with transformers, in: *Proceedings of the IEEE/CVF conference on computer vision and pattern recognition*, pp. 5557–5566.
- [20] Jha, D., Smedsrud, P.H., Riegler, M.A., Halvorsen, P., De Lange, T., Johansen, D., Johansen, H.D., 2020. Kvasir-seg: A segmented polyp dataset, in: *MultiMedia modeling: 26th international conference, MMM 2020, Daejeon, South Korea, January 5–8, 2020, proceedings, part II* 26, Springer. pp. 451–462.
- [21] Ji, G.P., Fan, D.P., Chou, Y.C., Dai, D., Liniger, A., Van Gool, L., 2023a. Deep gradient learning for efficient camouflaged object detection. *Machine Intelligence Research* 20, 92–108.
- [22] Ji, G.P., Fan, D.P., Xu, P., Zhou, B., Cheng, M.M., Van Gool, L., 2023b. Sam struggles in concealed scenes—empirical study on “segment anything”. *Science China Information Sciences* 66, 226101.
- [23] Ji, W., Li, J., Bi, Q., Liu, T., Li, W., Cheng, L., 2024. Segment anything is not always perfect: An investigation of sam on different real-world applications.
- [24] Khan, A., Khan, M., Gueaieb, W., El Saddik, A., De Masi, G., Karray, F., 2024. Camofocus: Enhancing camouflage object detection with split-feature focal modulation and context refinement, in: *Proceedings of the IEEE/CVF Winter Conference on Applications of Computer Vision*, pp. 1434–1443.
- [25] Kirillov, A., Mintun, E., Ravi, N., Mao, H., Rolland, C., Gustafson, L., Xiao, T., Whitehead, S., Berg, A.C., Lo, W.Y., et al., 2023. Segment anything, in: *Proceedings of the IEEE/CVF International Conference on Computer Vision*, pp. 4015–4026.
- [26] Le, T.N., Nguyen, T.V., Nie, Z., Tran, M.T., Sugimoto, A., 2019. Anabran network for camouflaged object segmentation. *Computer vision and image understanding* 184, 45–56.
- [27] Li, G., Yu, Y., 2016. Visual saliency detection based on multiscale deep cnn features. *IEEE transactions on image processing* 25, 5012–5024.
- [28] Li, Y., Zhang, X., Chen, D., 2018. Csrnet: Dilated convolutional neural networks for understanding the highly congested scenes, in: *Proceedings of the IEEE conference on computer vision and pattern recognition*, pp. 1091–1100.
- [29] Liang, Z., Wang, T., Zhang, X., Sun, J., Shen, J., 2022. Tree energy loss: Towards sparsely annotated semantic segmentation, in: *Proceedings of the IEEE/CVF conference on computer vision and pattern recognition*, pp. 16907–16916.
- [30] Liu, G., Wu, W., 2024. Search and recovery network for camouflaged object detection. *Image and Vision Computing* 151, 105247.
- [31] Liu, S., Liu, K., Zhu, W., Shen, Y., Fernandez-Granda, C., 2022a. Adaptive early-learning correction for segmentation from noisy annotations, in: *Proceedings of the IEEE/CVF Conference on Computer Vision and Pattern Recognition*, pp. 2606–2616.
- [32] Liu, X., Huang, X., 2024. Weakly supervised salient object detection via bounding-box annotation and sam model. *Electronic Research Archive* 32, 1624–1645.

- [33] Liu, Y., Li, H., Cheng, J., Chen, X., 2023. Mscaf-net: A general framework for camouflaged object detection via learning multi-scale context-aware features. *IEEE Transactions on Circuits and Systems for Video Technology* 33, 4934–4947.
- [34] Liu, Y., Wang, P., Cao, Y., Liang, Z., Lau, R.W., 2021. Weakly-supervised salient object detection with saliency bounding boxes. *IEEE Transactions on Image Processing* 30, 4423–4435.
- [35] Liu, Z., Deng, S., Wang, X., Wang, L., Fang, X., Tang, B., 2025. Ssfam: Scribble supervised salient object detection family. *IEEE Transactions on Multimedia* .
- [36] Liu, Z., Zhang, Z., Tan, Y., Wu, W., 2022b. Boosting camouflaged object detection with dual-task interactive transformer, in: 2022 26th International Conference on Pattern Recognition (ICPR), IEEE. pp. 140–146.
- [37] Lv, Y., Zhang, J., Dai, Y., Li, A., Liu, B., Barnes, N., Fan, D.P., 2021. Simultaneously localize, segment and rank the camouflaged objects, in: Proceedings of the IEEE/CVF conference on computer vision and pattern recognition, pp. 11591–11601.
- [38] Mei, H., Yang, X., Zhou, Y., Ji, G.P., Wei, X., Fan, D., 2023. Distraction-aware camouflaged object segmentation. *SCIENTIA SINICA Informationis (SSI)* 3, 7.
- [39] Pan, Y., Chen, Y., Fu, Q., Zhang, P., Xu, X., et al., 2011. Study on the camouflaged target detection method based on 3d convexity. *Modern Applied Science* 5, 152.
- [40] Pang, Y., Zhao, X., Xiang, T.Z., Zhang, L., Lu, H., 2024. Zoomnext: A unified collaborative pyramid network for camouflaged object detection. *IEEE transactions on pattern analysis and machine intelligence* .
- [41] Rahman, M.M., Marculescu, R., 2023. Medical image segmentation via cascaded attention decoding, in: Proceedings of the IEEE/CVF Winter Conference on Applications of Computer Vision, pp. 6222–6231.
- [42] Shi, W., Xu, J., Gao, P., 2022. Ssformer: A lightweight transformer for semantic segmentation, in: 2022 IEEE 24th International Workshop on Multimedia Signal Processing (MMSP), IEEE. pp. 1–5.
- [43] Song, L., Geng, W., 2010. A new camouflage texture evaluation method based on wssim and nature image features, in: 2010 International conference on multimedia technology, IEEE. pp. 1–4.
- [44] Tajbakhsh, N., Gurudu, S.R., Liang, J., 2015. Automated polyp detection in colonoscopy videos using shape and context information. *IEEE transactions on medical imaging* 35, 630–644.
- [45] Tang, L., Xiao, H., Li, B., 2023. Can sam segment anything? when sam meets camouflaged object detection. *arXiv preprint arXiv:2304.04709* .
- [46] Wang, L., Lu, H., Wang, Y., Feng, M., Wang, D., Yin, B., Ruan, X., 2017. Learning to detect salient objects with image-level supervision, in: Proceedings of the IEEE conference on computer vision and pattern recognition, pp. 136–145.
- [47] WANG, Q., HUANG, X., TONG, Q., LIU, X., 2023. Weakly supervised salient object detection algorithm based on bounding box annotation. *Journal of Computer Applications* 43, 1910.
- [48] Wang, W., Lai, Q., Fu, H., Shen, J., Ling, H., Yang, R., 2021a. Salient object detection in the deep learning era: An in-depth survey. *IEEE Transactions on Pattern Analysis and Machine Intelligence* 44, 3239–3259.
- [49] Wang, W., Xie, E., Li, X., Fan, D.P., Song, K., Liang, D., Lu, T., Luo, P., Shao, L., 2021b. Pyramid vision transformer: A versatile backbone for dense prediction without convolutions, in: Proceedings of the IEEE/CVF international conference on computer vision, pp. 568–578.
- [50] Wang, W., Xie, E., Li, X., Fan, D.P., Song, K., Liang, D., Lu, T., Luo, P., Shao, L., 2022. Pvt v2: Improved baselines with pyramid vision transformer. *Computational Visual Media* 8, 415–424.
- [51] Wang, X., Ding, J., Zhang, Z., Xu, J., Gao, J., 2024. Ipnnet: Polarization-based camouflaged object detection via dual-flow network. *Engineering Applications of Artificial Intelligence* 127, 107303.
- [52] Wei, J., Wang, S., Huang, Q., 2020. F³net: fusion, feedback and focus for salient object detection, in: Proceedings of the AAAI conference on artificial intelligence, pp. 12321–12328.
- [53] Woo, S., Park, J., Lee, J.Y., Kweon, I.S., 2018. Cbam: Convolutional block attention module, in: Proceedings of the European conference on computer vision (ECCV), pp. 3–19.
- [54] Xu, X., Chen, S., Lv, X., Wang, J., Hu, X., 2023. Guided multi-scale refinement network for camouflaged object detection. *Multimedia Tools and Applications* 82, 5785–5801.
- [55] Xu, X., Zhu, M., Yu, J., Chen, S., Hu, X., Yang, Y., 2021. Boundary guidance network for camouflage object detection. *Image and Vision Computing* 114, 104283.
- [56] Yan, Q., Xu, L., Shi, J., Jia, J., 2013. Hierarchical saliency detection, in: Proceedings of the IEEE conference on computer vision and pattern recognition, pp. 1155–1162.
- [57] Yan, X., Sun, M., Han, Y., Wang, Z., 2023. Camouflaged object segmentation based on matching–recognition–refinement network. *IEEE Transactions on Neural Networks and Learning Systems* .
- [58] Yang, C., Zhang, L., Lu, H., Ruan, X., Yang, M.H., 2013. Saliency detection via graph-based manifold ranking, in: Proceedings of the IEEE conference on computer vision and pattern recognition, pp. 3166–3173.
- [59] Yang, F., Zhai, Q., Li, X., Huang, R., Luo, A., Cheng, H., Fan, D.P., 2021. Uncertainty-guided transformer reasoning for camouflaged object detection, in: Proceedings of the IEEE/CVF international conference on computer vision, pp. 4146–4155.
- [60] Yang, Z., Choy, K., Farsiu, S., 2024. Spatial coherence loss for salient and camouflaged object detection and beyond. *arXiv preprint arXiv:2402.18698* .
- [61] Ye, Q., Zhou, Y., Huo, G., Liu, Y., Zhou, Y., Li, Q., 2024. Reverse cross-refinement network for camouflaged object detection. *Image and Vision Computing* 150, 105218.
- [62] Yin, B., Zhang, X., Fan, D.P., Jiao, S., Cheng, M.M., Van Gool, L., Hou, Q., 2024. Camoformer: Masked separable attention for camouflaged object detection. *IEEE Transactions on Pattern Analysis and Machine Intelligence* .
- [63] Yu, S., Zhang, B., Xiao, J., Lim, E.G., 2021. Structure-consistent weakly supervised salient object detection with local saliency coherence, in: Proceedings of the AAAI conference on artificial intelligence, pp. 3234–3242.
- [64] Yu, Z., Zhang, X., Zhao, L., Bin, Y., Xiao, G., 2024. Exploring deeper! segment anything model with depth perception for camouflaged object detection, in: Proceedings of the 32nd ACM International Conference on Multimedia, pp. 4322–4330.
- [65] Yue, G., Xiao, H., Xie, H., Zhou, T., Zhou, W., Yan, W., Zhao, B., Wang, T., Jiang, Q., 2023. Dual-constraint coarse-to-fine network for camouflaged object detection. *IEEE Transactions on Circuits and Systems for Video Technology* .
- [66] Zhang, J., Yu, X., Li, A., Song, P., Liu, B., Dai, Y., 2020. Weakly-supervised salient object detection via scribble annotations, in: Proceedings of the IEEE/CVF conference on computer vision and pattern recognition, pp. 12546–12555.
- [67] Zhang, J., Zhang, R., Shi, Y., Cao, Z., Liu, N., Khan, F.S., 2025. Learning camouflaged object detection from noisy pseudo label, in: European Conference on Computer Vision, Springer. pp. 158–174.
- [68] Zhang, Y., Li, K., Li, K., Wang, L., Zhong, B., Fu, Y., 2018. Image super-resolution using very deep residual channel attention networks, in: Proceedings of the European conference on computer vision (ECCV), pp. 286–301.
- [69] Zhang, Y., Zhou, T., Wang, S., Liang, P., Zhang, Y., Chen, D.Z., 2023. Input augmentation with sam: Boosting medical image segmentation with segmentation foundation model, in: International Conference on Medical Image Computing and Computer-Assisted Intervention, Springer. pp. 129–139.
- [70] Zhang, Z., Lin, Z., Xu, J., Jin, W.D., Lu, S.P., Fan, D.P., 2021. Bilateral attention network for rgb-d salient object detection. *IEEE transactions on image processing* 30, 1949–1961.

- [71] Zhao, J., Li, X., Yang, F., Zhai, Q., Luo, A., Jiao, Z., Cheng, H., 2024. Focusdiffuser: Perceiving local disparities for camouflaged object detection, in: European Conference on Computer Vision, Springer, pp. 181–198.
- [72] Zheng, P., Gao, D., Fan, D.P., Liu, L., Laaksonen, J., Ouyang, W., Sebe, N., 2024. Bilateral reference for high-resolution dichotomous image segmentation. CAAI Artificial Intelligence Research 3.
- [73] Zhu, H., Li, P., Xie, H., Yan, X., Liang, D., Chen, D., Wei, M., Qin, J., 2022. I can find you! boundary-guided separated attention network for camouflaged object detection, in: Proceedings of the AAAI conference on artificial intelligence, pp. 3608–3616.